Linköping University | ITN
Master's Thesis | Communication, Transport and Infrastructure
Autumn 2025 | LiU-ITN-TEK-A--25/068--SE

Conditions for and Prevention of Contrails in Swedish Airspace

— Modelling the Impact of Contrails in 2024

Tobias Elneros

Tutor: Lucie Havelka Smetanová
Examinator: Tatiana Polishchuk

LINKÖPINGS UNIVERSITET

Copyright

Upphovsrätt

Abstract

Condensation trails are the white line-shaped clouds that can appear after aircraft as their exhaust mixes with the ambient air. In certain conditions, these can survive for hours and develop into cirrus-like clouds. These are believed to be one of the largest contributors to non-CO_2 emissions from aviation, impacting global warming. They can have both a warming and a cooling effect, depending on the balance of inbound shortwave radiation and outbound longwave radiation. The net total is, however, a warming effect. Various mitigation strategies have been proposed. In this work, navigational avoidance by altitude adjustments is studied within the context of Swedish airspace. This is achieved by analysing historical flight trajectory data and meteorological data for the year 2024 using open-source contrail models, aircraft performance models, and aircraft trajectory optimisation models. Two contrail models — the Contrail Cirrus Prediction Model (CoCiP) and an algorithmic Climate Change Function (aCCF) from CLIMaCCF — are compared against each other. As expected, there are clear seasonal and diurnal effects, both regarding which altitudes that are contrail-prone, and which hours that see a net warming and net cooling effect. Geographical effects are more difficult to discern, especially due to the sharp decrease in air traffic north of 60°N. The relationship between navigational avoidance and other mitigation strategies is also discussed based on findings from related works.

Sammanfattning [Swedish]

Kondensationsstrimmor är de vita sträck på himlen som kan uppkomma efter flygplan när deras avgaser blandas med luft mättad på vatten. Under vissa förhållanden kan det ta flera timmar innan de åter förångas och innan dess hinner utvecklas till cirrusliknande moln. Dessa uppges vara bland de största bidragarna till flygets klimatpåverkande utsläpp. De kan ha en både positivt och negativt påverkande effekt beroende på balansen mellan den ingående och utgående strålning som reflekteras av dem. Summan är däremot att det tillförs energi till jordens energibudget. Flera motverkande strategier finns föreslagna. Strategin som undersöks i detta arbete är huruvida det går att undvika att skapa dessa kondensationsstrimmor genom att ändra flyghöjd ifall de bidrar till en ökning av energi. Historiska data för flygtrafiken och de meteorologiska förhållandena i svenskt luftrum analyseras för år 2024. Detta genomförs med öppet tillgängliga modeller för flygprestanda, skapandet av kondensationsstrimmor, och modeller för optimering av flygrutter. Två modeller för kondensationsstrimmor jämförs mot varandra: CoCiP och CLIMaCCF. Säsongsrelaterade och dygnsrelaterade förutsättningar framstår för vilka flyghöjder kondensationsstrimmor är mer sannolika samt när de har en positivt respektive negativt påverkande effekt. Skillnader i geografiska förutsättningar är svårare att urskilja, särskilt i beaktning av att mängden kommersiell flygtrafik norr om Arlanda är avsevärt mycket mindre än söder om. Samband mellan flyghöjdsändringar och andra motverkande strategier diskuteras utifrån relaterad forskning inom området.

Table of Contents

List of Figures

List of Tables

List of Abbreviations

aCCF	Algorithmic Climate Change Function
ADS-B	Automatic Dependent Surveillance-Broadcast System
ANN	Artificial Neural Network
API	Application Programming Interface
ARTP	Absolute Regional Temperature Change Potential
ATC	Air Traffic Controller
ATM	Air Traffic Management
ATR	Average Temperature Response
CC	Contrail-Creating (Segments)
CCF	Climate Change Function
CDF	Cumulative Distribution Function
CI	Cost Index
CoCiP	Contrail Cirrus Prediction Model
CTA	Control Area
CTR	Control Zone
DLR	Deutsches Zentrum für Luft- und Raumfahrt
EASA	European Union Aviation Safety Agency
ECAC	European Civil Aviation Conference
ECMWF	European Centre for Medium-Range Weather Forecasts
EF	Energy Forcing
ERA5	ECMWF Reanalysis v5
ERF	Effective RF
ETS	Equitable Threat Score
F-ATR	Future Emissions Scenarios Average Temperature Response
FIR	Flight Information Region
FL	Flight Level
GAM	Generalised Additive Model
GNSS	Global Navigation Satellite System
GTP	Global Temperature Potential
GWP	Global Warming Potential

IAGOS	In-service Aircraft for a Global Observing System
IATA	International Air Transport Association
ICAO	International Civil Aviation Organization
IFR	Instrumental Flight Rules
ISA	International Standard Atmosphere
ISS	Ice SuperSaturation
ISSR	Ice SuperSaturated Region
IWC	Ice Water Content
LS	Lower Stratosphere
MOZAIC	Measurement of Ozone and Water Vapour on Airbus In-Service Aircraft
MTOW	Maximum Take Off Weight
nvPM	Non-Volatile Particulate Matter
OLR	Outgoing Longwave Radiation
OpenAP	Open-Source Aircraft Performance Model
-.TOP	OpenAP Trajectory Optimizer
P-ATR	Pulse Emission Average Temperature Response
PS-Model	Poll–Schumann Model
QM	Quantile Mapping
RF	Radiative Forcing
RH_i	Relative Humidity with Regard to Ice
RVSM	Reduced Vertical Separation Minima
SAC	Schmidt–Appleman Criterion
SAF	Sustainable Aviation Fuel
TMA	Terminal Manoeuvring Area
UT	Upper Troposphere
UTC	Coordinated Universal Time
UTLS	Upper Troposphere and Lower Stratosphere

1. Introduction

Contrails, a portmanteau of *condensation trails*, can form as exhaust from aircraft mixes with ambient air. In certain conditions, depending on meteorology, aircraft, engine, and fuel properties, these can survive for several minutes and become known as persistent contrails, or develop further into contrail cirrus clouds lasting for hours. Their existence affects the balance of inbound shortwave radiation and outbound longwave radiation to the radiation budget of the Earth, and therefore contributes to global warming. This work studies historical flight trajectory data in combination with meteorological data from 2024 to evaluate the non-CO_2 climate impact of the aviation industry from contrails formed within Swedish airspace. To do this, this work utilises flight performance models and contrail evaluation models developed for this purpose: an Open-Source Aircraft Performance Model (OpenAP) and the Poll–Schumann Model (PS-model) for flight performance, and CoCiP and aCCF for contrail evaluation. Apart from analyses of the historical trajectories, a subset of flight trajectories is also optimised with the OpenAP Trajectory Optimizer (OpenAP.TOP), with an objective function that includes a cost grid of contrail impact derived from CoCiP and the fuel burn from OpenAP. This master's thesis is based on the findings from a literature survey on the subject by Bohman Axelsson, Elneros and Jerreling (2025), which includes the author of this work.

1.1. Delimitations

This study is limited to flight trajectory data above 9500 feet within Swedish airspace in 2024. Only flights for which the aircraft typecode is known have been included. The dataset has been further restricted to turbofan-powered aircraft typically used in commercial aviation, excluding turboprop, piston, and military aircraft. The typecodes represented in the final dataset are shown in *Figure 6*.

2. Thesis Purpose

Avoiding the formation of contrails is regarded as a potential measure for the aviation industry to reduce its contribution to global warming. This work uses state-of-the-art models available as open source to quantify the effect of contrails created within Swedish airspace and investigate whether this could have been mitigated through altitude adjustments.

3. Research Questions

1. Under what conditions do aircraft create persistent contrails?
2. How can the impact of contrail-forming flights be quantified?
3. To what extent can persistent contrails be mitigated through altitude adjustments?

4. Background

The background of this work provides an overview of the current understanding of the effects that contrails have on climate change, a brief overview of mitigation policies and challenges referencing Bohman Axelsson et al. (2025), some brief concepts related to air navigation that are relevant to this work, the three main criteria or characteristics of contrail creation, development and effect — i.e. the Schmidt–Appleman criterion (SAC), ice supersaturated regions (ISSR), and radiative forcing (RF) — descriptions of the models used in this work, and information regarding the data sources together with uncertainties related to these.

4.1. Condensation Trails

The following subsections address the three criteria required for persistent warming contrails to be formed: the Schmidt–Appleman criterion for contrail creation, the ice supersaturated regions for contrail persistency, and the third criterion regarding the balance of radiative forcing that determines whether a contrail will be warming or cooling.

4.1.1. Schmidt–Appleman Criterion

The Schmidt–Appleman criterion is named after the works of Schmidt (1941) and Appleman (1953) and was further developed by Schumann (1996). For contrails to initially form, the SAC requires that the relative humidity with respect to water reaches 100 % as the ambient air mixes with exhaust from aircraft.

4.1.2. Ice Supersaturated Regions

The ice supersaturated regions allow for contrails to not dissipate within a few minutes or seconds and thereby become persistent. Two definitions of a persistent contrail exist in the literature. The first definition is that the post-wake vortex ice water content (IWC) is greater than $10^{-12}\ kg\ kg^{-1}$ (Teoh et al., 2024a). The second definition is that they last longer than ten minutes (Kärcher, 2018). Defining for the ISSRs is that the relative humidity with respect to ice reaches or exceeds 100 % (Gierens et al., 2020; Hofer et al., 2024).

4.1.3. Balance of Radiative Forcing

To determine whether a contrail will have a warming or cooling effect involves many uncertainties. As discussed by Rosenow and Fricke (2023), it is difficult to evaluate both the inbound and outbound RF. A simplified explanation is that a contrail is considered warming if the contrail reflects more radiation back to the Earth than it hinders and reflects back into space. While the RF is instantaneous — measured in $W\ m^{-2}$ — a contrail can evolve and last from a few seconds up to several hours while varying in size. A subsequent consideration is which timeframe to use in the evaluation of the climate effect of increased emissions from additional fuel burn, as the effect of contrails is instantaneous while the effect of carbon dioxide and nitrogen oxides exists over a long period of time (Lee et al., 2021; Dietmüller et al., 2023). This is covered further in *Section 4.4*.

4.2. Mitigation Strategies

In the literature survey on contrails by Bohman Axelsson et al. (2025), four major mitigation strategies were identified: navigational avoidance, alternative fuels, new engine architectures, and financial incentives. The main mitigation strategy analysed in this work is navigational avoidance through altitude adjustments. The alternative fuels strategy is also brought up for the discussion in *Section 8* considering findings in *Section 5.3* from related works.

Navigational avoidance includes vertical and horizontal route adjustments. While avoiding ISSRs decreases the risk of producing a persistent contrail, it will likely increase the fuel burn and overall operational cost as flight planning is often based on a cost index (CI), which is a trade-off between fuel costs and the cost of time (Bohman Axelsson et al., 2025; Gao, 2013).

Alternative fuels, apart from potentially being more environmentally friendly themselves, can affect the creation of contrails depending on their chemical composition and the quantity of emitted condensation nuclei. While hydrogen-based fuels emit more water, the produced water droplets are thought to be fewer and larger, and therefore less persistent (Megill & Grewe, 2025). The topic of fuel in relation to contrail creation is also covered in *Section 5.3*.

New engine architectures, apart from those adapted to alternative fuels, could be designed such that the exhaust is cooled before being mixed with the ambient air, or so that the air and fuel are mixed prior to ignition in a lean-burn system which lowers particulate emissions (Bohman Axelsson et al., 2025; Rolls-Royce, 2018).

Financial incentives are currently non-existent with regard to contrails. While there is no direct monetary cost for producing contrails, producing warming contrails comes with a social cost. There have been suggestions to create a contrail tax or to implement a green route-charging system (Bohman Axelsson et al., 2025; Bolić et al., 2024; Gao, 2013). In 2025, the European Union is implementing a monitoring, reporting and verification scheme to evaluate the non-CO_2 effects of aviation. The results are expected to be presented by the end of 2027 and thereafter assessed to determine whether legislative proposals can be made (Quante et al., 2025; European Commission, 2025). This is criticised by the Director General of IATA, the International Air Transport Association, which argues that there is insufficient humidity data to accurately predict when contrails will be produced and, among other points, suggests the Commission to fund installation of humidity sensors on aircraft (Walsh, 2024).

4.3. Meteorological Data

Historical weather data is available from the European Centre for Medium-Range Weather Forecasts (ECMWF). Specifically, the ECMWF Reanalysis v5 (ERA5) data is used in this work. This contains hourly meteorological data in a $0.25° \times 0.25°$ grid from several pressure levels, or for certain variables at the surface level (Hersbach et al., 2023a,b).

To validate the ERA5 data, researchers have compared it with in-situ measurements from the MOZAIC and IAGOS programmes (Petzold et al., 2015), where commercial aircraft have been specially equipped with meteorological sensors to collect more accurate data. Reutter et al. (2020) found that the fraction of ISSR in the IAGOS data was similar to ERA5 if the ERA5 ISS relative humidity with respect to ice (RH_i) threshold was 95 % in the uppermost troposphere, 90 % at the tropopause, and decreasing to below 85 % up into the lowermost stratosphere where both fractions become practically 0. The tropopause is the boundary between the troposphere and the stratosphere, and aircraft often have their cruise phase in the lower stratosphere (Petty, 2008). The typical tropopause height varies with latitude and appears between 29 000 to 36 000 feet between latitudes 55°N and 70°N (Kuzmin et al., 2025). The upper troposphere and lower stratosphere can be abbreviated to UT and LS, respectively, or together as UTLS.

4.3.1. Humidity Correction

This section explains the need for humidity correction and summarises some existing methods based on findings from Bohman Axelsson et al. (2025).

Gierens et al. (2020) and Reutter et al. (2020) have found that the ERA5 data underestimates the RH_i when comparing with in-situ measurements from the IAGOS and MOZAIC programmes. This also leads to an underestimation of persistent contrail occurrences. There have been several approaches to mitigate this problem. One simple approach is to set the threshold of supersaturation to e.g. 90 or 95 % instead of 100 % (Petzold et al., 2020). Schumann (2012) also discusses the resolution of meteorological data, and how there can be supersaturated areas within a grid cell that on average is subsaturated, thus also inferring the need for a lower threshold value.

To compare the agreement between ERA5 data and the in-situ measurements, Gierens et al. (2020) introduced the equitable threat score (ETS) to the field. An ETS of 1 indicates perfect agreement, an ETS of 0 indicates a random relation, and an ETS below 0 indicates an inverse relationship. They compared results for the SAC and for ISS in January, April, July and October, and found that the ETS for ISS in July was as low as 0.05 while the ETS for ISS in January was 0.25. For the SAC, the ETS was 0.55 and 0.85 for July and January, respectively. Given that the SAC determines whether contrails are created, they conclude that this can be forecasted quite reliably. However, the ISS which determines contrail persistency cannot be forecasted reliably solely from ERA5 data. Therefore, there have been several attempts to improve this data.

Several early studies with CoCiP implemented a simple conversion by applying a factor of 0.95^{-1} to the RH_i (Teoh et al., 2024a).

Teoh et al. (2022a) scaled the RH_i by dividing with a coefficient a. If the result was above 1, the RH_i was further scaled to the power of coefficient b and capped at 1.65. For the ERA5 HRES, the values of a and b were found by minimising the Cramér von Mises test statistic measuring the fit of two empirical distributions, resulting in $a = 0.9779$ and $b = 1.635$. This formula was developed further by Teoh et al. (2024a) to account for latitude and thus also additionally includes an ambient temperature parameter. The 2022 version of this method is referred to as *T22* in other published papers (cf. Hofer et al., 2024; Wolf et al., 2025).

Wolf et al. (2025) propose a quantile mapping (QM) method, which essentially creates cumulative distribution functions (CDF) from the ERA5 and the IAGOS data. A given ERA5 datum is compared with the ERA5 CDF and thereafter substituted with the corresponding quantile value of the IAGOS CDF. Wolf et al. (2024) found the effects of applying this method to be minor and 'argued that ERA5 performs well in terms of the statistical representation of ISSR and [persistent contrail] occurrence'.

Hofer et al. (2024) attempted to use a generalised additive model (GAM) to retrieve a corrected RH_i from various combinations of parameters and found a version with five parameters to work the best. They also compared the results of using this GAM where the ERA5 RH_i had been corrected using the method by Teoh et al. (2022a) and where it had been corrected with the QM method presented in the preprint to Wolf et al. (2025). They note that using the quantile mapping results in saturation being reached at an RH_i of 0.934 in ERA5.

Platt et al. (2024) also use quantile mapping, and in addition apply a shift-and-stretch calibration by Eckel et al. (2012) such that the variance between ERA5 ensemble members matches the variance between the ERA5 ensemble mean and IAGOS measurements.

Wang et al. (2025) apply an artificial neural network (ANN) to correct the ERA5 RH_i and found a significant improvement compared to the statistical methods by Wolf et al. (2025) and Teoh et al. (2022a).

The resulting ETS of these methods can be seen in *Table 1*, in comparison to IAGOS data. While the quantile mapping and T22-method both do improve the ERA5 data as intended, as shown by the increase of the ETS, the ANN appears superior.

Table 1: ETS scores of various methodologies correcting ERA5 data to match in-situ measurements from IAGOS.

Paper	ERA5	T22	QM	ANN	Comment
Hofer et al. (2024)	0,198	0,248	0,344		ISS without GAM
	0,378 [1]	0,376	0,377		ISS with GAM
Wolf et al. (2025)	0,27	0,35	0,36		SAC AND ISS
	0,51	0,53	0,54		SAC AND NOT ISS
	0,19	0,23	0,24		ISS AND NOT SAC
Platt et al. (2024)	0,179		0,291		ISS without Stretch
			0,241		ISS with Stretch
Wang et al. (2025)	0,14			0,52	ISS Clear and Cloudy LS
	0,06			0,47	ISS Clear-Sky UTLS
	0,21			0,70	ISS Cloudy UTLS
	0,23			0,71	ISS Clear and Cloudy UT

4.4. Climate Metrics

Various metrics for the effect that contrails have on climate change appear in the literature, including average temperature response (ATR), CO_2-equivalents (CO_2e), global temperature potential (GTP), global warming potential (GWP), absolute regional temperature change potential (ARTP), radiative forcing (RF), effective radiative forcing (ERF), and energy forcing (EF) (Dietmüller et al., 2023; Lee et al., 2021; Lund et al., 2017; Teoh et al., 2022a).

ATR, GTP and GWP include a time horizon over which the effects are considered, such as 20, 50 or 100 years. ATR gives a metric of temperature in Kelvin (Dietmüller et al., 2023), while GTP and GWP give ratios to CO_2e and 'are the most commonly applied metrics' (Lee et al., 2021). The ATR metrics can also differ between pulse emission (P-ATR) and future emission scenarios (F-ATR). P-ATR assumes a one-time instantaneous release of emissions at a specific point in time, such as the immediate climate impact of a single flight. F-ATR assumes a continuing or growing stream of emissions and therefore represents what the climate impact will be if flights continue to create contrails in the same manner (Dietmüller et al., 2023). Lund et al. (2017) have explored the ARTP concept which considers regional impacts, as opposed to the global focus of GWP and GTP, and found that 'ARTP illustrate important differences in the latitudinal patterns of [RF] and temperature response', but note that the concept requires better consideration of vertical distributions.

[1] Note that this value is for ERA5 with GAM, and not solely ERA5 as the rest in this column.

Meanwhile, RF, ERF, and EF are based on the resulting energy balance in the atmosphere, with the unit $W\ m^{-2}$ for RF and ERF. 'RF is commonly used for assessing the climate impact of contrails' (Schumann, 2012). Dietmüller et al. (2023) write that RF has a 'linear relationship to the steady-state global mean near-surface temperature change' but also mention how this fails for heterogeneous distributions like contrails, in comparison to homogeneous distributions like CO_2. This is what the ERF accounts for. To assess this, an efficacy parameter which compares the contrail effect with the effect of CO_2 can be used. The efficacy parameter is the ratio between the ERF and RF. Based on studies by Ponater et al. (2005), Rap et al. (2010), and Bickel et al. (2020), which found the efficacies to be 0.59, 0.31, and 0.35, respectively, Lee et al. (2021) used a contrail efficacy of 0.42. For CO_2, the ERF to RF ratio is 1. EF is the instantaneous RF multiplied by the area of a contrail — from its width W and length L — and integrated over time t, as seen in *Equation (1)*, resulting in a measure of energy given in Joules.

$$EF = \int RF(t) * W(t) * L(t)\ dt \quad (1)$$

To compare the effects of contrail-creating flight segments, the EF can advantageously be normalised per distance or time to get a measure of force or power for comparable analyses.

4.5. Flight Trajectory Data

Aircraft localisation can be performed through several methods. One widely used system today is the Automatic Dependent Surveillance-Broadcast system (ADS-B). It uses Global Navigation Satellite System data (GNSS) to retrieve the position of the aircraft, which it thereafter transmits twice per second. The signals are picked up by receivers which can be stationed on the ground or carried by other aircraft. The transmission builds on an upgrade to the already existing Mode-S technology, which simplified the deployment of the ADS-B system as Mode-S transponders have been mandated since 1993 (Schäfer et al., 2014). In Europe, ADS-B has been mandated for larger aircraft since 2023 (EASA, 2020).

Apart from its direct functionality to the aviation industry, ADS-B has enabled live air traffic tracking services like FlightAware (2025) and Flightradar24 (2025), where the latter has existed since 2006, has over 40 000 receivers, but is still lacking global ADS-B coverage. These sites do not, however, give open access to the raw ADS-B data, which is the reason for the development of OpenSky (Schäfer et al., 2014). Similarly to FlightAware and Flightradar24, OpenSky consists of a network of ADS-B receivers. The data received by the OpenSky receivers is stored in a database that is openly available for research purposes, and it is this database that is used to source historical flight trajectories in this work. The data include values such as timestamps with corresponding altitude, latitude, longitude, and the unique icao24 address of the transmitting aircraft. This does, however, require that the transmissions from aircraft can be picked up by a receiver, and the data availability therefore depends on the coverage of the receiver network. With a substantially extended network since the first OpenSky receivers in central Europe in 2014, there are still areas where sufficient coverage is missing. The OpenSky coverage in 2024 can be seen in Sun et al. (2024).

4.6. Airspace and Air Navigation

Altitude in aviation is derived from air pressure rather than a vertical distance. As the air pressure can vary spatiotemporally, this is given with reference to the standard pressure of 1013.2 hPa above the so-called transition altitude such that all aircraft fly with reference to the same pressure. The pressure altitude is then also referred to as a flight level (FL), where a flight level is a hundredth of the pressure altitude in feet such that FL095 is equivalent to

9500 feet in standard pressure. Below the transition altitude, where the vertical position in relation to the ground is more important, the altitude is given with reference to the pressure at the mean sea level (ICAO, 2018; Falkenby, 2016). In this work, altitude is given in reference to the standard pressure. As already mentioned in *Section 4.3*, the meteorological data are also given for pressure levels.

Aircraft are required to keep a minimum separation from one another. To maintain vertical separation, they are assigned different altitudes or flight levels. Below FL290, the vertical separation is 1000 ft, otherwise it is 2000 ft unless reduced vertical separation minima (RVSM) rules apply. If RVSM rules apply, the vertical separation is 1000 ft also between FL290 and FL410 (ICAO, 2005). RVSM rules apply above FL285 in Swedish Airspace (LFV, 2022) where aircraft typically must fly according to instrumental flight rules (IFR) (LFV, 2019a). During the cruise phase of an IFR flight, aircraft flying a magnetic track between 000° and 179° shall maintain odd-thousand-foot altitudes, and between 180° and 359° even-thousand-foot altitudes, up to FL410 above which the 2000 ft separation is in effect again (ICAO, 2005; LFV, 2021).

Swedish airspace, or the Swedish flight information region (FIR), is a so-called free-route airspace along with most of the European airspace. Here, routes can be freely planned between defined entry and exit points while remaining subject to air traffic control (EUROCONTROL, 2025). The airspace extends from the ground and is vertically unlimited. Laterally, the Swedish FIR is defined by lines between coordinates over water or along the national borders to Norway, Finland and Denmark. Notably, the Danish island of Bornholm lies within the Swedish FIR. While the Swedish FIR is divided into various types of airspace (e.g. uncontrolled Class G airspace, CTR, TMA, CTA), the higher altitudes where contrails have the potential to be created from airliners in their cruising phase are within the Swedish control area (CTA). Apart from having a floor at FL125 over the Scandinavian mountain range to the northwest, the CTA is bounded between FL095 and FL660 (LFV, 2019b).

4.7. Aircraft Performance Models

To evaluate the fuel flow and subsequent emissions from aircraft, the aircraft performance must be modelled using the given flight trajectories. Two openly available models have been identified and used within this work: the PS-model, and OpenAP.

4.7.1. The PS-Model

Poll and Schumann (2021a, 2021b, 2025) have presented in their series of three papers the development of a method for the scientific community to estimate fuel burn and other performance parameters during climb, cruise, initial descent, and holding. This for 67 aircraft types defined by their ICAO designation. Apart from an ICAO designation, it requires an aircraft trajectory, the variation of atmospheric temperature with atmospheric pressure, and wind speed components. They have compared the performance of their model to flight data recorders from actual flights and concluded that their residual root mean square error is less than two per cent. The model can easily be used together with CoCiP in the pycontrails library (Shapiro et al., 2025).

In their first paper in the series of three, Poll and Schumann (2021a) present the modelling of the fuel burn from, as they call them, governing equations and relations based on a constant Reynolds number, from fluid dynamics. An expression for the Reynolds number is derived from an analysis of a parameter found to capture atmospheric effects in combination with the

International Standard Atmosphere (ISA). Thereby, through power-law approximations and order-of-magnitude estimates, they acquired explicit relations for key quantities. In the second paper (Poll & Schumann, 2021b) they extend the model to also include engine thrust and engine overall efficiency, which are important parameters in the modelling of contrail creation. To apply the model for a specific aircraft, eight parameters are needed. Some of these are not openly available and have therefore been estimated through aerodynamic theory and data correlations from empirical studies. In the third paper (Poll & Schumann, 2025) — while the first two considered the cruise phase of a flight — the model is extended to also include take-off, initial climb, climb, descent, holding, approach, and landing, which covers most normal operations of a commercial aircraft.

4.7.2. OpenAP

Sun et al. (2020) have developed the open aircraft performance model (OpenAP) which, similarly to the PS-Model, is intended to provide the scientific community with an open-source model, in contrast to licensed proprietary models, that can provide aircraft and engine properties, kinematic and dynamic performances, and a set of utility libraries. It currently contains properties of 36 aircraft and 417 engines. Most relevant to this paper is the modelling of fuel flow, which is part of the dynamic performances. It is calculated with a third order polynomial with three fuel flow coefficients from the ICAO aircraft engine emissions databank. These affect the ratio of the thrust over the max thrust within the three orders, where the max thrust is from the same databank, and the thrust can be calculated by OpenAP. An additional term for the calculation of the fuel flow also considers that it increases with altitude for the same thrust level. The thrust is calculated within a four-degrees-of-freedom point-mass motion model which can be expressed as six ordinary differential equations.

4.8. Contrail Evaluation Models

There have been several approaches to modelling contrails, with varying foci. This paper focusses on models that can simulate the creation, development, and effect of contrails from individual flights with the prospect of being implemented in the flight planning process. Other examples of models include those modelling the aggregated effect on weather and climate change, such as modules of Global Circulation Models (cf. Burkhardt & Kärcher, 2009; Chen et al., 2012; Chen & Gettelman, 2013; Bock & Burkhardt, 2016; Burkhardt et al., 2018) or models like APCEMM (Fritz et al., 2020) that calculate the atmospheric chemical response for contrails. In the literature survey on contrails by Bohman Axelsson et al. (2025), two models were found to fit the purpose of this paper, namely CoCiP and a contrail aCCF. CoCiP is available through the pycontrails Python library, which also includes an interface to the CLIMaCCF library in which the contrail aCCF is found (Shapiro et al., 2025).

The two models have in common that they take gridded meteorological data as input, e.g. from ECMWF, along with flight trajectories defined by four-dimensional waypoint vectors with latitude, longitude, altitude, and time. In practice, the altitude is pressure altitude or a flight level which depends on the pressure, as mentioned in *Section 4.6*.

4.8.1. CoCiP

CoCiP, a Contrail Cirrus Prediction model, was initially created and developed by Schumann (2010; 2012) and Schumann et al. (2012a) at Deutsches Zentrum für Luft- und Raumfahrt (DLR). CoCiP has since been developed into two branches. One branch remains at DLR, while the branch available in pycontrails has been further developed by Imperial College and

Breakthrough Energy. While originally written in Fortran, the pycontrails branch has been translated to MATLAB and subsequently further developed in Python (Engberg et al., 2025).

The meteorological data provided as input to the model are linearly interpolated to the relevant location and time. The data needed can be seen in *Table 2* in *Section 6.1*. Humidity can be interpolated differently (Schumann, 2012). While metrics such as temperature have a near-linear lapse rate, thus allowing for linear interpolation, this is not the case for humidity, which instead has an exponential lapse rate. If the humidity is linearly interpolated, this can introduce an overestimation between two known data points. Therefore, it is possible to use a cubic-spline interpolation in CoCiP, or to interpolate in the logarithmic domain (Breakthrough Energy Foundation, 2025). The four-dimensional waypoints of the flight trajectory can also be interpreted in consecutive pairs as flight segments, and the altitude is converted to the static pressure. The initial contrail creation also depends on several aircraft parameters: wingspan, mass, true air speed, fuel consumption, soot number emission index, and the overall engine propulsion efficiency (Schumann, 2012).

The SAC determines whether a contrail is initially formed. If two consecutive waypoints satisfy the SAC, the flight segment in between is accompanied by one or more contrail segments. Ice supersaturation is not an explicit criterion within CoCiP (Schumann, 2012).

To simulate the contrails, CoCiP makes use of a Gaussian plume model derived from Konopka (1995), which considers both turbulent diffusion and shear (Schumann, 2012). Schumann states that the ‘shape of aged contrails is sometimes not too far different from a Gaussian plume shape […] However, the initial exhaust jet, wake vortex and contrail (with primary and secondary parts) often deviate considerably from this shape’ (Schumann, 2012). The initial lack of accuracy in the model is, however, defended by the fact that it is the persistent contrails that have a significant impact on the climate, and the initial properties are instead estimated by a parametric model.

A contrail is defined by state vectors in space and time, with static pressure, plume parameters, ice mass content, and the number of ice particles. The displacement of a contrail directly after its creation is simulated by a parametric wake vortex model, which considers the effect of the wake from the aircraft. The parameters are derived from a model by Holzäpfel (2003). This gives the initial depth, width, and maximum and mean downward displacements. A few seconds into the contrail lifetime, the temperature increase from combustion heat and sublimation is considered small enough to consider the temperature of the contrail and the ambient air to be the same, which allows the ice mass content to be computed from thermodynamics. Within the wake phase, some of this disappears due to adiabatic warming as the pressure increases. The initial number of ice particles is modelled to depend on the soot emission index and fuel consumption, while it is also mentioned that other sources, such as volatile materials, can have an effect, albeit smaller. The number of ice particles in the step after the wake phase is assumed to decrease in proportion to the corresponding ice mass content. However, Schumann (2012) also discusses that they evolve differently in practice and that lower ratios for the number of ice particles do appear. If the initial creation of the contrail segment is iteration 0, the iteration after the wake vortex model is iteration 1. Based on the work by Unterstrasser (2016), the pycontrails version of CoCiP has since been developed to allow for the inclusion of a parameterised model of the ice crystal survival fraction in the wake-vortex phase (Engberg et al., 2025).

It is assumed that the aircraft wake does not affect the displacement in the subsequent contrail evaluation iterations, i.e. those after the wake vortex phase. Here, the contrail evolution is modelled with a Lagrangian model that uses a Runge-Kutta scheme of two to six iterations for the positional variables, followed by a sub-model that considers the effect of turbulence. The other variables are numerically integrated while also considering that the contrail segment length can change with time. The Gaussian plume model is also adapted to consider the variation in segment length, where the horizontal plume changes inversely to the segment length. The cross-section area in the Gaussian Plume model changes depending on shear, and horizontal and vertical diffusivities (Schumann, 2012).

The ice water content evolution depends on whether the ambient air is supersaturated or not. In supersaturated ambient air, the ice water content increases, and vice versa. The speed at which this occurs depends on the temperature. The sublimation of the contrail also depends on ice particle loss, which in CoCiP is simulated by three sub-models: 'plume-internal turbulence, […] sedimentation-induced aggregation, […] losses induced by turbulent humidity fluctuations by mesoscale turbulence and gravity waves […] and possibly plume turbulence' (Schumann, 2012). The contrail optical depth depends on the plume dimensions and a radiation extinction factor which in turn depends on the density of the air and ice, the effective radius of particles which in turn depend on their shape, or habit, and an efficiency factor from approximate Mie theory (cf. Horvath, 2009). The last factor describes how light scatters off spherical particles depending on the refractive index of ice, the wavelength of light, and on the effective radius of particles. Radiative heating of the contrail is also mentioned as a possible source of ice particle loss (Schumann, 2012; Schumann et al., 2012).

The computation of RF is divided into two parametric models, one for longwave spectral ranges, which contributes with positive values, and one for shortwave spectral ranges, which contributes with negative values. In turn, these models are calculated for various particle habits that give the corresponding RF in a weighted sum. Both longwave and shortwave radiation depend on the particle effective radius, optical depth of the contrail, and the optical depth of cirrus above the contrail. The longwave RF also depends on the temperature and the outgoing longwave radiation retrieved from the meteorological data. The shortwave RF also depends on the reflected solar radiation, solar direct radiation, and the solar constant. The cosine of the solar zenith angle is derived from the ratio of the solar direct radiation and the solar constant (Schumann, 2012; Schumann et al., 2012).

Schumann (2012) discusses the flaws of the model and potential improvements, such as the effect of radiative heating on thick long-lived contrails or the effect of assuming ice saturation and equilibrium inside the contrail on contrails with low ice particle concentrations. The overarching quality strongly depends on the input data, and the choice of threshold value and interpolation for humidity data. The radiative heating effect has since been worked further upon, and CoCiP can now take this into consideration. Engberg et al. (2025) mention how this is based on the equivalent implementation to the DLR version of CoCiP, however, it is written in the pycontrails code (Shapiro et al., 2025) that the implementation is based on personal communication and that there is no scientific article that discusses the equations. Schumann and Heymsfield (2017), and Jensen et al. (1998) are mentioned as giving the rationale to include this effect.

Other developments include the finding that the non-volatile particulate matter activation rate depends on the difference between the ambient and SAC threshold temperatures (Bräuer et

al., 2021; Engberg et al., 2025). An option to consider contrail overlapping has also been developed (Teoh et al., 2024a), however, it is not enabled in this work.

While CoCiP was created to simulate contrails given a flight trajectory as input, Engberg et al. (2025) developed a grid-based version to evaluate contrail developments at discrete points in a spatiotemporal grid. The intent is that a grid could be used to include contrail costs for flight trajectory optimisers or to create polygons of airspace to avoid due to a high warming potential. Some parameters known to the trajectory version are lost when simulating contrail effects with the grid version. This includes the angle of the contrail segments in relation to the wind, which instead is a calibrated constant, and the fuel flow rate and efficiency, which are estimated with a grid-adapted variant of the PS-model.

Rosenow and Fricke (2023) mention that CoCiP only reflects the time of day on the solar zenith angle, that 'Optical properties are only parameterized for radiant fluxes which have already been integrated over a hemisphere' (Rosenow & Fricke, 2023) and claim that 'no angular dependence due to the time of day or the spatial orientation of the contrail can be taken into account' (Rosenow & Fricke, 2023). However, in a comparison between the grid and trajectory version in Engberg et al. (2025), it appears that a simplification from the trajectory version to the grid version is indeed the loss of consideration of the orientation of the contrail, which affects the spreading rate, ice crystal loss rate, and lifetime of the contrail. Rosenow and Köhler (2024) also mention that CoCiP neglects factors that affect contrail lifetime and optical properties, citing Schumann and Heymsfield (2017).

4.8.2. CLIMaCCF

CLIMaCCF has been developed by Dietmüller et al. (2023). It makes use of algorithmic climate change functions (aCCFs) by van Manen and Grewe (2019) to provide future near-surface temperature change for various emissions (e.g. CO_2, NO_x) in a spatiotemporal resolution, which have been converted to Kelvins per kilogram of fuel. They are based on the computationally heavier climate change functions (CCFs) from a global atmospheric chemistry-climate model system. The introduction of a contrail aCCF to obtain the equivalent contrail effects was made by Yin et al. (2023). Even if simplifications have been necessary, it has been shown that the 'aCCFs are in broad agreement with the climate change metric of earlier studies' (Dietmüller et al., 2023). It is noted that it is still a prototype that was designed with regard to the North Atlantic in summer and winter and that they do not recommend its use for spring and autumn or tropical regions. Currently, aircraft types are aggregated into three classes in CLIMaCCF: regional, single-aisle (narrowbody) and widebody. However, the aircraft type does not appear to be a parameter for the contrail-specific aCCFs (Dietmüller et al., 2023; Yin et al. 2023).

While discussing the efficacies for various emissions and attributed values, with 0.42 for contrails, these efficacy values are not accounted for in aCCF by default in the CLIMaCCF library. There is, however, an option to use those by Lee et al. (2021) (Dietmüller et al., 2023; Dietmüller & Simorgh, 2023), and they are used by default if using the pycontrails interface for aCCF (Shapiro et al., 2025). CLIMaCCF consists of seven aCCFs: for water vapour (H_2O), carbon dioxide (CO_2), ozone (O_3), methane (CH_4), primary-mode ozone (PMO), nighttime contrails, and daytime contrails. The ozone and methane aCCFs depend on the NO_x emissions. The contrail aCCFs 'estimates the global- and annual-mean specific RF per flight distance using the parametric equation of Schumann et al. (2012)' (Yin et al. 2023) and is converted to P-ATR20 with a constant factor of 0.0151 that was found with the climate response model AirClim. It has been found that nighttime RF correlates with temperature and

therefore depends on the 4D temperature data. Daytime RF, on the other hand, depends on the outgoing longwave radiation (OLR), which is also required in the meteorological data per lateral position and time. This also requires that the conditions for contrail creation are met in order to multiply the flight distance with the potential contrail coverage (Yin et al. 2023).

The contrail evolution is described in the supplement to Yin et al. (2023) by Klingaman and Shine. They used the parametric equations of Schumann et al. (2012) to derive the aCCFs for contrails. The contrail trajectory is given by a fourth-order Runge-Kutta integration scheme in a model by Methven (1997) as developed by Irvine et al. (2014). However, the lifetime of the contrail does not consider sedimentation and dissipation. The contrail width, length, and lifetime are also assumed to be constant, where the width is 200 metres, the length is the square root of the grid area used in the model, and the lifetime is six hours. The lifetime of six hours is justified as 'a reasonable assumption given that 92% of contrails have lifetime of up to 6 hours' (Yin et al., 2023, Supplementary Material). This means that the ATR20 of contrails with a shorter lifetime is typically overestimated, and vice versa for contrails lasting longer than six hours. The contrail optical depth is given by an extinction coefficient by Unterstrasser and Gierens (2010), and the ice water content as well as the ice particle effective radius by Schumann et al. (2017). As the scattering properties also depend on the shape of the ice particles, known in the literature as habits, they also consider this effect on the effective radius after Schumann et al. (2011). The RF of nighttime contrails was found to fit an exponential regression of temperature ($R = 0.73$), and the RF of daytime contrails a linear regression of OLR ($R = 0.86$). As the nighttime RF depends on temperature, and temperature decreases with altitude in the troposphere, this results in RF being modelled as decreasing towards higher altitudes during nighttime. As previously mentioned, the net RF per flight distance from the functions of temperature and OLR is multiplied by a factor of 0.0151 to obtain the resulting P-ATR20 (Yin et al., 2023, Supplementary Material).

Two versions of aCCF exist, aCCF-V1.0, and aCCF-V1.0A, where the former version calibrated to the climate response model AirClim results in the latter version (Dietmüller et al., 2023). The former version is used in this work.

4.9. Optimisation

The OpenAP.TOP flight trajectory optimiser by Sun (2022) models the flight with state vectors that include flight state variables for lateral position, altitude and mass, and control state variables for Mach number, vertical rate and heading. These are given various path constraints and flight performance constraints. To discretise the continuous problem, each flight segment is divided into equally spaced collocation points, between which the state vectors are approximated using polynomials. The objective cost is retrieved by integrating the objective function dependent on the polynomially approximated state vectors over the flight segment. The problem is thereafter solved with the symbolic optimisation framework CasADi and the interior point solver MUMPS. There are five trajectory optimisation cases available: one for climb, cruise, and descent, respectively; one for a complete flight which considers all phases at once; and one for a complete flight which optimises the first three cases individually and combines them into a multiphase complete flight. There is also a set of objective functions prepared for use to minimise either fuel consumption, time, cost index, or the climate impact models GWP and GTP over 20, 50 or 100 years. The GWP and GTP consider CO_2, H_2O, NO_x, SO_x, and soot, but they do not consider any potential effects from the creation of contrails. The OpenAP Handbook (Sun, 2025) provides information on how to construct cost grids, with examples of cost grids based on contrails, and how to implement meteorological data to account for the wind components.

5. Related Work

This work is based on findings in the literature survey *A Literature Survey on Aviation Contrails* by Bohman Axelsson, Elneros, and Jerreling (2025), which includes approximately 80 sources related to the modelling of contrails, optimisation, or the underlying data. This section covers further topics related to this work, including seasonality in *Section 5.1*, cooling contrails in *Section 5.2*, the influence of aircraft type, engine type, fuel type, and mass in *Section 5.3*, and air traffic management in *Section 5.4*. What is covered in this Related Work section is more relevant for the analyses of the results and the discussion, while the background is more relevant for the methodology section.

The findings in the literature study include the works by Schmidt (1941) and Appleman (1953) on what is today known as the Schmidt-Appleman Criterion stating the requirements for contrail formation, which has been further developed by Schumann (1996). One question posed in the literature survey was which models that exist for contrail prediction, which had been similarly asked and answered by Martín Frías et al. (2024). CoCiP and CLIMaCCF were found to best fit the purpose of this work. Schumann (2010) created the first version of CoCiP, which has since been developed by Schumann (2012) and Schumann et al. (2012). While initially requiring a flight trajectory as input, it now also exists as a grid-based model (Engberg et al., 2025). The CoCiP and CoCiP Grid models are now available through the Python library pycontrails (Shapiro et al., 2024) through which an interface to CLIMaCCF by Dietmüller et al. (2023) is also available. These models have been covered in *Section 4.8*.

5.1. Seasonality

Dischl et al. (2022) performed a study on the seasonality of potential contrail coverage over central Europe. This was conducted for three pressure levels of historical ECMWF ERA5 data using the SAC for a set of parameters and RH_i thresholds of 80 % and 95 %. They also considered using meteorological data from the National Centers for Environmental Prediction but favoured ERA5 as it has a higher vertical and lateral resolution, and because it had been proven to agree well with in-situ measurements for H_2O data. With the seasons divided into sets of calendar months (DJF, MAM, JJA, SON), they found that there is a higher potential for persistent contrails in winter and autumn when considering their entire geographical range at 34 000 feet due to lower temperatures and higher humidity. In southern Sweden, below 60°N, the potential appears larger in summer and autumn. Within Sweden, the lowest potential appears in winter below 65°N and in spring above 65°N. They explain the low potential in the north in spring as being due to lower humidity. For western Europe, the potential for persistent contrails along with its standard deviation appears to be the lowest in the summer months, with July in particular, for all three studied altitudes. The variation is larger for the remaining seasons. The trend does, however, vary between the altitudes.

5.2. Cooling Contrails

While much literature on the effect of contrails focusses on the warming persistent contrails, Rosenow and Fricke (2023) dedicated a paper to the cooling contrails. Apart from the solar zenith angle, they also examined the effect of the azimuthal angle. They found that solar zenith angles at 70°–80° provide the largest cooling effect as the likelihood of the radiation to be scattered back upwards is larger for these angles while the solar intensity remains sufficiently high. At 50°N, it is true for the solar zenith angle to be within this range for practically the whole day in November, December, and January, but only for an hour in the rest of the months. At 60°N, it is true for the whole day in February and October, never true

in the winter months between, and true for one to four hours in the rest of the year. At 70°N, it is true for the whole day in October, and presumably at some point in February–March which does not show due to how the data is discretised, while it is never true in November through February, and true for six hours per day from March to September. They also found that the net effect is significantly worse above snow and ice than over any other surface type.

Rosenow and Köhler (2024) therefore investigate how long contrails live in relation to the position of the sun, and the conditions for this, to determine whether they are net cooling or warming. They found that thin ISS layers and a small upward wind allowed the contrails to survive just long enough to maintain a cooling effect and that these conditions exist in 30 % of the year in northern latitudes. This was also more common at 200 hPa (approximately 38 500 feet) than 300 hPa (approximately 30 000 feet). This was noted while acknowledging that lateral movements were not considered and that ISS thickness is difficult to validate.

5.3. Aircraft Type, Engine Type, Fuel Type and Mass

A couple of articles have studied the effect of aircraft types on contrail creation. Understrasser and Görsch (2014) studied simulations of aircraft types of six different sizes, ranging between a regional airliner (CRJ) and the largest passenger aircraft in the world (A380). To remove the effect of engine type and fuel type, they assumed a constant ice crystal emission index. They found little difference between aircraft types at an RH_i of 100 % and 140 %. However, at 120 % RH_i, larger aircraft had a proportionally larger decrease in ice crystal numbers during the vortex phase, albeit the largest aircraft had approximately an order of magnitude more than the regional jet initially. The contrail depth became twice as large for the A380 compared to the CRJ. Combined, they used the concept of total extinction to determine the significance of a contrail, which is the disturbance of shortwave flux or the product of optical thickness and contrail width. They found that the A380 had 1.5–2.5 times higher total extinction than the CRJ. Jeßberger et al. (2013) studied both contrails probed behind Airbus A319, A340, and A380 aircraft in the same meteorological conditions, and also simulated global air traffic with the A319 and A380 using CoCiP. In the simulation, they found that the RF from A380 aircraft was approximately 3.5 times larger than for the A319. For the probed contrails, they found that the optical depth was thrice as large for the larger aircraft. The effective particle diameters were found to be indifferent. The total extinction was found to have a linear relationship with fuel flow, while the relationship to RH_i was non-linear. Sussmann and Gierens (2001) studied the difference between aircraft with two and four engines, including the positioning of the engines and the proximity to the vortex cores. While contrails never completely dissipated until after the vortex phase for aircraft with four engines, they link this primarily to the higher fuel flow of the studied aircraft. They did, however, find that for stronger vortices, the effect of enhanced mixing with accelerated ice evaporation was stronger than the effect of delayed ice evaporation by the vortex cores.

Aircraft with the same typecode can also be equipped with different engine types with different characteristics. One of these is the emission of non-volatile particulate matter, which is correlated with the ice crystal number and optical depth of contrails as it acts as condensation nuclei (Teoh et al., 2022b, 2024b). While this can vary greatly between engines for different aircraft linked to aircraft type characteristics, or by orders of magnitude for the same engine in different flight phases, it can also vary greatly between engines for the same aircraft type during the same flight phase. The discrepancies appear larger for aircraft types that are offered with engines from multiple manufacturers, such as the A320, A20N and B78X (Teoh et al., 2024b, Supplementary Material). The engine type is not transmitted via ADS-B signals. Therefore, Teoh et al. (2022a) used a commercial database to obtain the

engine type through the aircraft registration, which was available for 79 % of jet aircraft in their dataset of global air traffic. For the remaining aircraft, they used the engine with the largest market share. Sun (2022) shows how the engine type for an A320 aircraft can affect the results of route optimisation.

Voigt et al. (2021) analysed the results from tests probing the emissions of an A320 flying with different fuels. These were ordinary Jet A1 (100 %), a blend of Jet A1 with a synthetic kerosene component from the Fischer–Tropsch process (59:41), and two different blends of Jet A1 with bio-based kerosene from plant oil (51:49 and 70:30) where the Jet A1 also had 'different aromatic and naphthalene contents' (Voigt et al., 2021). They found that the synthetic blend resulted in a 50 % soot reduction, and a slightly lower and higher reduction for the two bio-based blends. They also analysed the results for the apparent ice crystal number emission index, which showed a reduction of approximately 50 % for the synthetic and the first bio-based blends, and a reduction of approximately 75 % for the second bio-based blend. While analysing alternative fuels, the study also highlights how the composition of the Jet A1 fuel can have a significant impact, implying that classifying the fuel type as Jet A1 might not be sufficiently detailed for contrail studies. The study did, however, not include the results for 100 % Jet A1 of the type used in the second bio-based blend. Burkhardt et al. (2018) state that 'using a 50:50 blend of an alternative fuel and Jet A fuel [can lead] to a reduction in [RF] of about 21 %'.

Using CoCiP, Teoh et al. (2022b) found that using sustainable aviation fuels (SAF) over the North Atlantic resulted in a higher occurrence of persistent contrails. However, due to lower nvPM emissions, they were found to last a shorter time with a lower width and optical depth, resulting in a 30 % decrease in EF for a 50:50 blend, and a 45 % decrease with 100 % SAF. Acknowledging the current limited supply of SAF, they first suggest that targeting flights in winter and at night could maximise the benefits of using SAF for contrail mitigation. Given that contrails produced with SAF last shorter, contrails produced late at night might not survive to also have cooling effects in the morning, but contrails produced in the afternoon can disappear before only the warming effect remains. Looking at the potential decrease in EF rather than targeting those with the highest EF could therefore be better. A 99:1 blend of conventional aviation fuel and SAF for all flights would result in a 0.6 % decrease in annual EF, while a 50:50 blend for two per cent of flights with the highest decrease in EF compared to conventional fuel would result in a 10 % decrease in annual EF. A higher blend of SAF for even fewer flights would not continue to increase the benefit. Given the uncertainties in modelling and real-time operations, they suggest that a 90:10 blend for the ten per cent of flights with the highest decrease in EF could hedge the benefits of SAF to a decrease in annual EF of 5 %.

Quante et al. (2025) performed a study with 84 demonstration flights between Stockholm and Copenhagen using a 35:65 blend of conventional and renewable fuel in aircraft equipped with LEAP-1A26 engines. They also simulated the flights with CoCiP for various fuel blends, although with the CFM56-5B4 engine type instead of the one on the actual aircraft and with different CoCiP settings from those used in this work. The use of a real engine with lower nvPM emissions (cf. Teoh et al., 2024b, Supplementary Material) than the simulated one likely affected the results of their comparison with satellite imagery. 28 simulated flights produced contrails, of which 21 were partially covered by clouds, and the remaining seven were not analysed further. The modelling gave a decrease in EF of 10.22 % by using the demonstration fuel blend compared to the conventional average which aligned with the fuel used at the two airports at the time. A 50:50 blend resulted in a 23.23 % decrease in EF. They

also compared this with a low hydrogen version of conventional fuel, which resulted in a 12.81 % *increase* in EF. Overall, they proved that it is possible to establish the logistics for short- to medium-range flights by providing the fuel to the largest airport in Sweden and refuel the aircraft at remote stands with refuelling trucks. However, they argue that the infrastructure required to provide targeted refuelling options for long-range aircraft would be costly, albeit less than what would be required to introduce hydrogen fuel technology.

The aircraft mass is also an important parameter to consider. Poll and Schumann (2025) state that fuel flow is directly proportional to mass during the cruise phase of a flight (in steady, straight and level cruise), with a stronger and weaker dependency during climb and descent, respectively. The mass also affects the service ceiling, or reachable altitude, of the aircraft. Sun (2022) shows how the initial aircraft mass can affect the results of route optimisation.

5.4. Air Traffic Management

Baneshi et al. (2023) took the trajectory optimisation from a single flight perspective to a network perspective for air traffic management (ATM), as the avoidance of ISSRs can lead to an increased complexity with a greater need for conflict avoidance and increased workload for air traffic controllers (ATC). They used aCCFs to quantify the impacts of various emissions and direct optimal control to retrieve the individually optimised trajectories for a set of flights over the Iberian Peninsula using both cost and climate impact as alternative objectives. Thereafter a resolution algorithm and simulated annealing with a neighbourhood generator function were used to optimise at the network level. They found that accepting a three per cent increase in cost could reduce the climate impact by 28 %, but at the same time increase the number of conflicts by 65 %. For cost-optimised routes, 80 % of conflicts were resolvable by speed adjustments while only 25 % were resolvable for the climate-impact-optimised routes. Suggesting that this could increase by also adjusting the flight paths and departure times, Baneshi et al. (2024) thereafter employed a 4D optimiser for the ECAC airspace. They found that moving from cost-optimised trajectories to climate-impact-optimised trajectories led to generally lower cruising altitudes, but also lower Mach numbers, the latter being attributed to lower NOx emissions. For their weighting of operational costs, an F-ATR20 improvement of 27–38 % led to an eight per cent increase in costs, while a two per cent increase in costs enabled a 21–30 % improvement. However, this leads to a change from a nearly uniform distribution of flight altitudes to a preference for lower altitudes with a significant increase in ATM conflicts. More recently, Baneshi et al. (2025) also used multi-agent deep reinforcement learning for conflict resolution and saw an improvement of over 100 % in F-ATR20 for a cost increase of only 2.5 %, meaning that the net effect went from warming to slightly cooling for their dataset of flights between 12 and 14 UTC the day before the 2018 winter solstice.

6. Methodology

The methodology consists of four main parts: data acquisition and preparation, contrail modelling, optimisation, and the definition of seasons used within this work.

6.1. Meteorological Data

The meteorological data variables required by CoCiP and aCCF are presented in *Table 2* (Shapiro et al., 2025). Data was acquired for the period 2024-01-01–2025-01-02, pressure levels 750–125 hPa, and a lateral extent of 35°N–90°N and 25°W–60°E. The pressure levels correspond to approximately 8 000–48 000 feet, and the lateral extent represents the approximate bounds of the Swedish FIR ± 20° latitude and ± 40° longitude to allow for contrail advection. The data was acquired from ECMWF and stored locally in GRIB format, as illustrated in *Figure 1*, amounting to 187 GB of meteorological data.

Table 2: The meteorological variables required by aCCF and CoCiP.

Variable Name	Short Name	Domain	Used in Model(s)
Geopotential	z	Pressure Levels	aCCF & CoCiP
Fraction of Cloud Cover	cc	Pressure Levels	CoCiP
Potential Vorticity	pv	Pressure Levels	aCCF
Relative Humidity	r	Pressure Levels	aCCF
Specific Cloud Ice Water Content	ciwc	Pressure Levels	CoCiP
Specific Humidity	q	Pressure Levels	aCCF & CoCiP
Surface Solar Radiation Downwards	ssrd	Surface Level	aCCF
Temperature	t	Pressure Levels	aCCF & CoCiP
Top Net Solar Radiation	tsr	Surface Level	CoCiP
Top Net Thermal Radiation	ttr	Surface Level	aCCF & CoCiP
U Component of Wind	u	Pressure Levels	aCCF & CoCiP
V Component of Wind	v	Pressure Levels	aCCF & CoCiP
Vertical Velocity	w	Pressure Levels	CoCiP

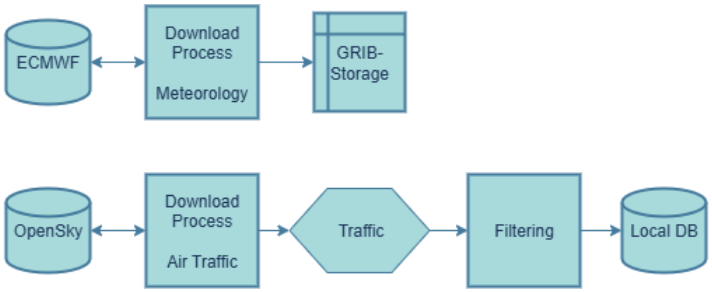

Figure 1: A schematic of the data acquisition.

6.2. Flight Trajectories

Trajectory data was retrieved from the OpenSky historical database through its API for the year 2024 and the bounding box of Swedish airspace. The data was handled as Traffic and Flight objects from the Traffic library by Olive (2019), which distinguishes individual flights by the combination of their callsign, icao24-address, and time between data points. This was thereafter filtered before being stored in the local database, as illustrated in *Figure 1*. Irrelevant columns and duplicate rows were removed, and waypoints outside an

approximation of the Swedish FIR were discarded. Traffic retrieves the typecode of the aircraft for a particular flight from the OpenSky aircraft database on the icao24 address. If this does not yield a typecode, an alternative option is to manually retrieve it from, for example, airframes.org (2025), if available. The typecodes were analysed to determine whether the flights were by commercial turbofan aircraft and if the typecodes are represented in the flight performance models. Flights by turboprops, piston aircraft, gyroplanes, gliders, balloons, helicopters, military aircraft, aircraft that are typically private jets or business jets, and aircraft for which the typecode could not be identified were discarded. The remaining trajectories were filtered to remove vertical and lateral spikes, flights that did not reach 20 000 feet, waypoints below 9 500 feet, i.e. waypoints below the floor of the Swedish CTA, and flights with a duration of less than 180 seconds. The trajectories were finally resampled to ten seconds before being added to the local database. Information about discarded flights, except their trajectories, was also stored.

Pairs of trajectories with the same icao24 address and the same callsign that both had waypoints within an hour of each other were further analysed to determine whether they were likely to be the same flight. This could result in the two trajectories being joined into one, both being kept, one being discarded or two being discarded. There were three main reasons for joining two trajectories, one being that the flight flew too long outside of coverage, which appears to occur mainly over Jämtland, Småland, and the Baltic Sea, the second being that the flight left and re-entered Swedish airspace which typically occurs along the western and eastern borders, and the third reason being that intermediate waypoints were not available within the threshold leading into the next hour during the hour-wise processing of the raw data. There was one main reason for keeping two trajectories, which is where a flight appeared to have landed, either due to a diversion or being a flight with multiple legs (e.g. ADD–ARN–OSL or HEL–ARN–BGO). The decision to discard one of the trajectories, or even both, is when it appears that there is erroneous data that had been missed by the filter, which could be for various reasons. At times, one trajectory resembled a flightpath while the other did not. It could also be that both resembled flightpaths, at times roughly one-hour apart along the same path. If one included more waypoints than the other, this was kept. Otherwise, the earlier of the two was kept as time zone errors could be a cause of erroneous data. If both resembled flightpaths but not along the same path, however sometimes appearing to be mirrored, the one that appeared more plausible for the given callsign was kept, alternatively the one that appeared to follow common flight routes.

6.3. Contrail Modelling

After acquiring the meteorological data from *Section 6.1* and flight trajectory data from *Section 6.2*, the data was processed hourly with CoCiP and CLIMaCCF.

For air traffic with their first waypoint in a given hour, the trajectories were processed as illustrated in *Figure 2*. Information regarding the trajectories was retrieved from the database and the latest final waypoint among the trajectories was noted. The meteorological data covering up to a potential contrail duration of twenty-four hours for the final waypoint was loaded into the CoCiP model. The contrail integration parameter indicating the time steps to evaluate the contrail evolution was set to 5 minutes after recommendations by Engberg et al. (2025). The relative humidity correction was set to a constant humidity scaling with a threshold of 95 %. As seen in *Section 4.3.1*, other potentially better methods exist, however this method was used to avoid having the meteorological data input as a source of variation for comparison between CoCiP and aCCF. This was also the reason why the option to calculate the P-ATR20 as a result from the CoCiP model was enabled. The resulting

P-ATR20 values were multiplied by 0.42 to account for the efficacy as implemented in the pycontrails interface to the aCCF model. The cubic-spline method was used for humidity interpolation, and the linear interpolation was used for the other meteorological variables. The options to consider radiative heating effects and enhanced ice survival fraction in the wake vortex phase were enabled. The PS-model was set to evaluate the aircraft performance, primarily due to the availability of data for more aircraft types compared to OpenAP, and secondarily because CoCiP has built-in support for the model. The resulting fuel flow data for each waypoint was saved for future use with aCCF. Thereafter, with the typecode of the aircraft and the trajectory data, CoCiP was set to evaluate whether any contrails had been created. The results were saved to the local database, both per the flight trajectory waypoints used as input, and per resulting waypoint of the resulting contrail segments themselves as they move with the wind. Two important parameters that the model can consider were unknown, these were the engine type of a specific aircraft, and the initial mass. The PS-model therefore uses engine parameters that are average values for engine types available for the given typecode and assumes an initial mass of 0.8 MTOW. For some typecodes that are not available within the PS-model, substitute typecodes of aircraft with similar characteristics were used instead.

For aCCF, the interface within pycontrails is used to access the model. The flight trajectory data and the meteorological data were loaded as described for CoCiP in the paragraph above, as also seen in *Figure 2*. The fuel flow data from the PS-model performance evaluation within CoCiP was retrieved as well. The interpolation methods for humidity and for the other meteorological variables were also equally set to cubic-spline and linear, respectively. The ISSR RH_i threshold was set to 0.95 %. The persistent contrail formation area was set to depend on the SAC, and not on the ISSR only. The option to receive the aCCF results in Kelvin per kilogram fuel was enabled. The pycontrails aCCF interface enables the option to consider an efficacy of 0.42 by default. Thereafter, also using the typecode of the aircraft and the trajectory data, aCCF was set to evaluate the climate effects of the flight. This returned the results for each aCCF in P-ATR20, which were multiplied by the fuel flow and segment duration to retrieve the results in Kelvin. These were thereafter stored along the flight waypoints within the local database.

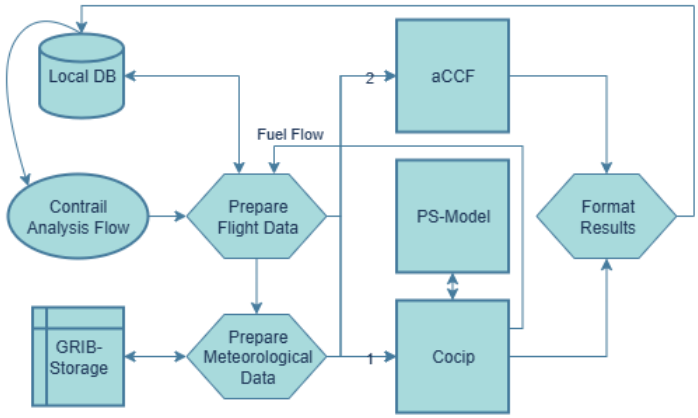

Figure 2: A schematic of the contrail simulation process.
The output of the box preceded by a 1 is required as input to the box preceded by a 2.

6.4. Optimisation

The cruise-phase optimiser and complete-flight optimiser from OpenAP.TOP were adapted to optimise two classes of flights: overflights and full flights. For overflights, the entire original trajectory is above an altitude of 20 000 feet and thereby determined to be suitable for the cruise-phase optimiser. For full flights, the first and last waypoints are both below an altitude of 14 000 feet, and thereby determined to include a climb, cruise, and descent phase, which is suitable for the complete-flight optimiser. In addition to the original OpenAP.TOP model formulations, the waypoints were constrained to the same lateral coordinates as the original flight trajectory, the initial and final waypoints were also constrained to the same altitude, the maximum time was constrained to 1.10 times the original duration, and original constraints affecting the heading were removed.

CoCiP Grid was used with the same data and settings as the trajectory version, as presented in *Section 6.3*, to generate a cost grid of P-ATR20 values in Kelvin, which was adapted to fit the format of the optimiser. An objective function was constructed as the sum of the cost grid and the fuel consumption from the state variable, where the fuel consumption was also converted to P-ATR20 in Kelvin. A wind field was also derived from the meteorological data and adapted and enabled for the optimiser. With the mass being unknown, the optimiser was run for masses of 0.50 through 0.90 of MTOW in increments of 0.10 to increase the chances of at least one successfully optimised trajectory. The successfully optimised trajectories were thereafter analysed with the trajectory version of CoCiP with the same parameters as used for the initial flight, including a default initial mass of 0.8 MTOW. The optimised trajectory with the lowest resulting EF was saved to the local database. While the initial contrail simulation had been performed for flights on an hourly basis in *Figure 2*, the optimisation analysis described above, and shown below in *Figure 3*, was performed on a per-flight basis.

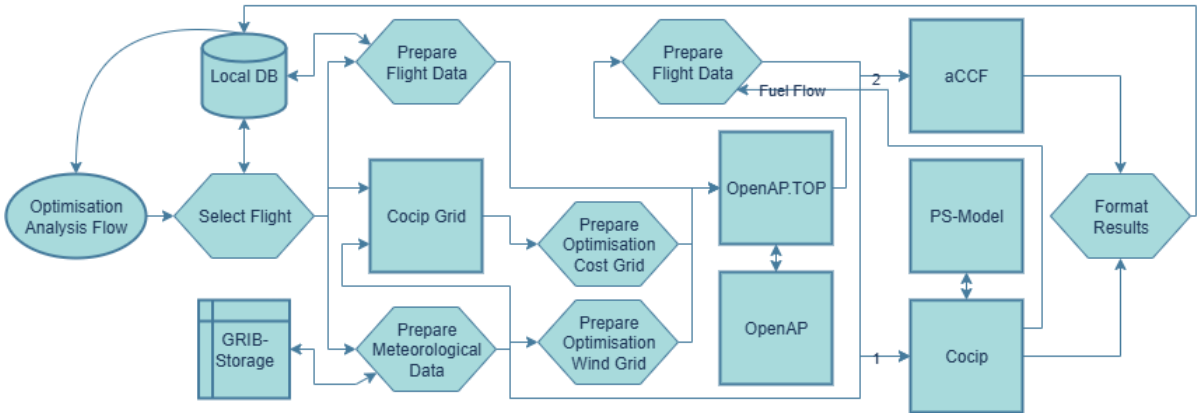

Figure 3: A schematic of the optimisation process.

6.5. Definition of Seasons

Given that the effect of contrails varies with the solar zenith angle, the seasons were defined to be centred on the solstices and equinoxes to capture the effects of varying daylight at the studied latitudes. This is shown in *Table 3*. Days and hours are given in UTC, meaning that local solar time is + 20 min / 5° longitude. The average local time for traffic in Swedish airspace is UTC+01:03:29.

Table 3: The definition of the seasons used within this work, centred on the solstices and equinoxes.

Season	Start	Midpoint	End
Winter	2024-01-01 2024-11-05	Winter Solstice 2024-12-21	2024-02-03 2024-12-31
Spring	2024-02-04	Spring Equinox 2024-03-20	2024-05-05
Summer	2024-05-06	Summer Solstice 2024-06-20	2024-08-04
Autumn	2024-08-05	Autumn Equinox 2024-09-22	2024-11-04

7. Results

The results include *Section 7.1* which presents the dataset, *Section 7.2* which presents the results with regard to latitude, longitude, altitude, time of day, and season, *Section 7.3* which analyses the results for the 16 most common aircraft typecodes identified in the dataset and presented in *Figure 6*, and *Section 7.4*, which presents the optimisation results.

7.1. Flight Data

The filtering of the OpenSky flight trajectory data from within the Swedish FIR in 2024 resulted in 677 698 individual flights as identified by the Traffic library. 93 039 were discarded because a typecode could not be identified from the icao24 address. 113 203 were discarded because the typecode did not belong among the studied aircraft types, such as turboprop and piston aircraft, helicopters, gyroplanes, gliders, balloons, smaller turbofan aircraft typically used in general aviation (e.g. private jets and air ambulances), and aircraft primarily used for military purposes. 37 673 were discarded because they did not pass the trajectory filtering. 35 425 were discarded because they did not reach altitudes above 20 000 feet, 569 were discarded because they lasted less than three minutes within the CTA. 1167 were discarded due to being merged with another Traffic flight, resulting in 584 new flights. 185 were discarded after manual analysis of flight pairs with identical icao24 addresses and callsigns within an hour of each other. The resulting dataset for contrail studies therefore consists of 397 022 flights. The flight trajectories are sampled into ten-second flight segments. The lateral geographical distribution of the dataset is shown per season in *Figure* 4. The vertical distribution per latitude and longitude and per season is shown in *Figure 5*.

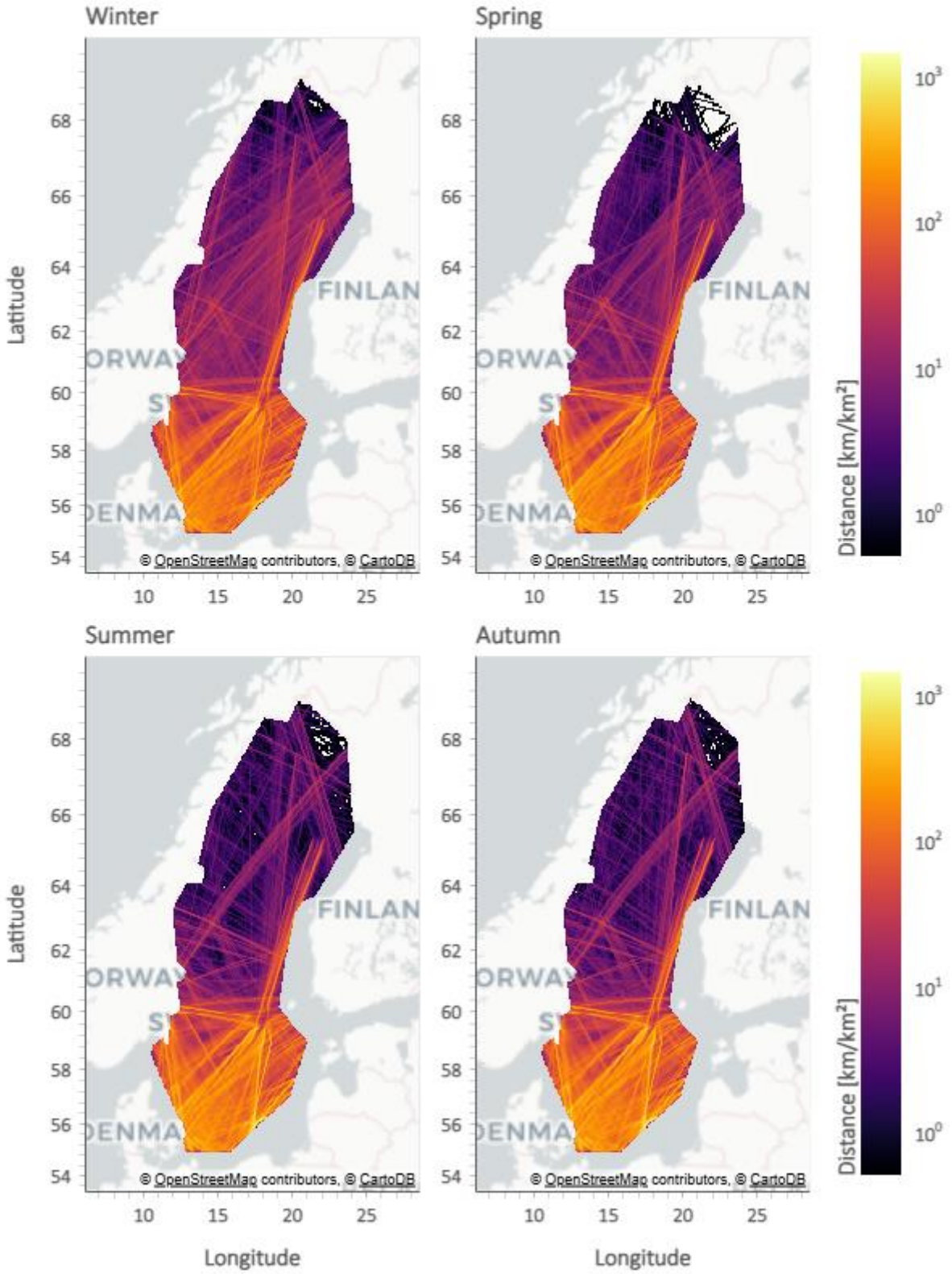

Figure 4: The lateral geographical extent of the dataset studied, per season.

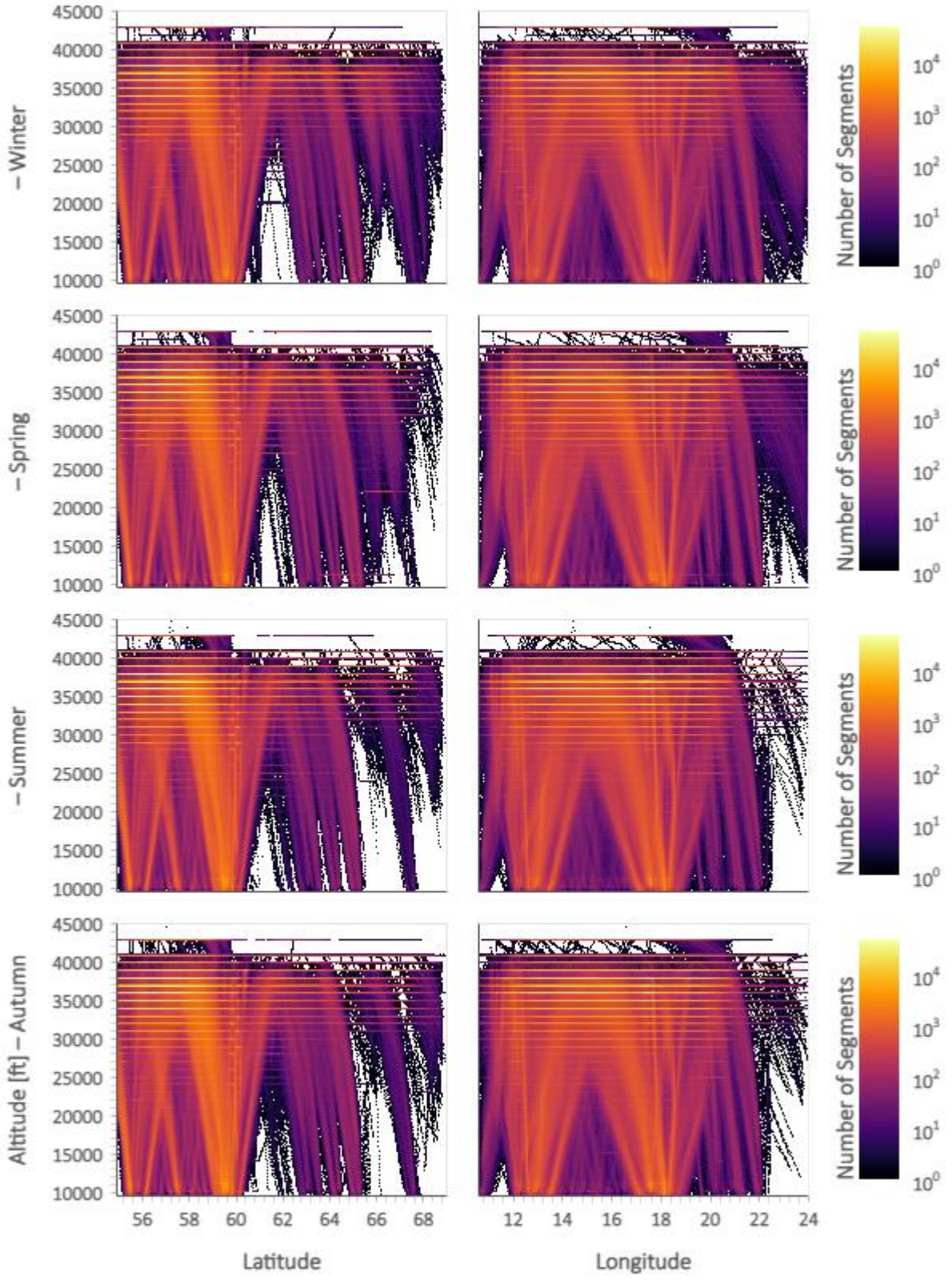

Figure 5: The vertical extent of the dataset per latitude, longitude, and season.

As expected, much of the Swedish traffic appears to radiate to or from the capital region, with most of the traffic remaining south of 60°N. North of this, there are the clear north–south domestic routes, some more clearly defined east–west overflights, and two less well-defined diagonal overflight-paths. There appear to be more freely routed flights descending into or climbing out of Finland during the winter and spring seasons. Notably, there is also significant traffic routing around the border of Kaliningrad airspace. The 65 identified aircraft typecodes within the dataset, and the distance flown by each, are shown in *Figure 6*. Note that the distance axis is logarithmic.

7.2. Spatiotemporal Contrail Distribution

The metric used to measure the effect of contrails in the Results section is primarily the EF without the efficacy parameter, often normalised by segment length in kilometres. The results for the contrail aCCF are converted from P-ATR20 to EF using the formula from the pycontrails library, including the exclusion of the efficacy parameter. The results can be from either flight segments or contrail segments. The flight segments are parts of the trajectories flown by the aircraft, sampled at ten-second intervals. If a flight segment produces a contrail, these flight segments are called contrail-creating (CC) or contrail-forming flight segments. A contrail segment related to the contrail-forming flight segment is then also created. These have a lifetime of five minutes each, after which a new evolved contrail segment is created until the contrail has completely dissipated. A flight segment can therefore have either none or several contrail segments related to it.

In comparison with *Figure 4*, the lateral spatial coverage of contrail formation, as modelled with CoCiP and expressed as a percentage, is shown in *Figure 7*. This shows that contrails are more likely to form in winter than in summer. From these figures, it is difficult to draw any conclusions regarding potential effects on latitude, given the smaller dataset for northern latitudes and the longitudinal distribution. The lower percentages near the Scandinavian capitals are likely due to traffic in climb and descent below contrail-forming altitudes. With a relatively large amount of data, there appears to be a slightly greater likelihood of contrail formation over the Baltic at 55°N–58°N in the autumn, winter and spring.

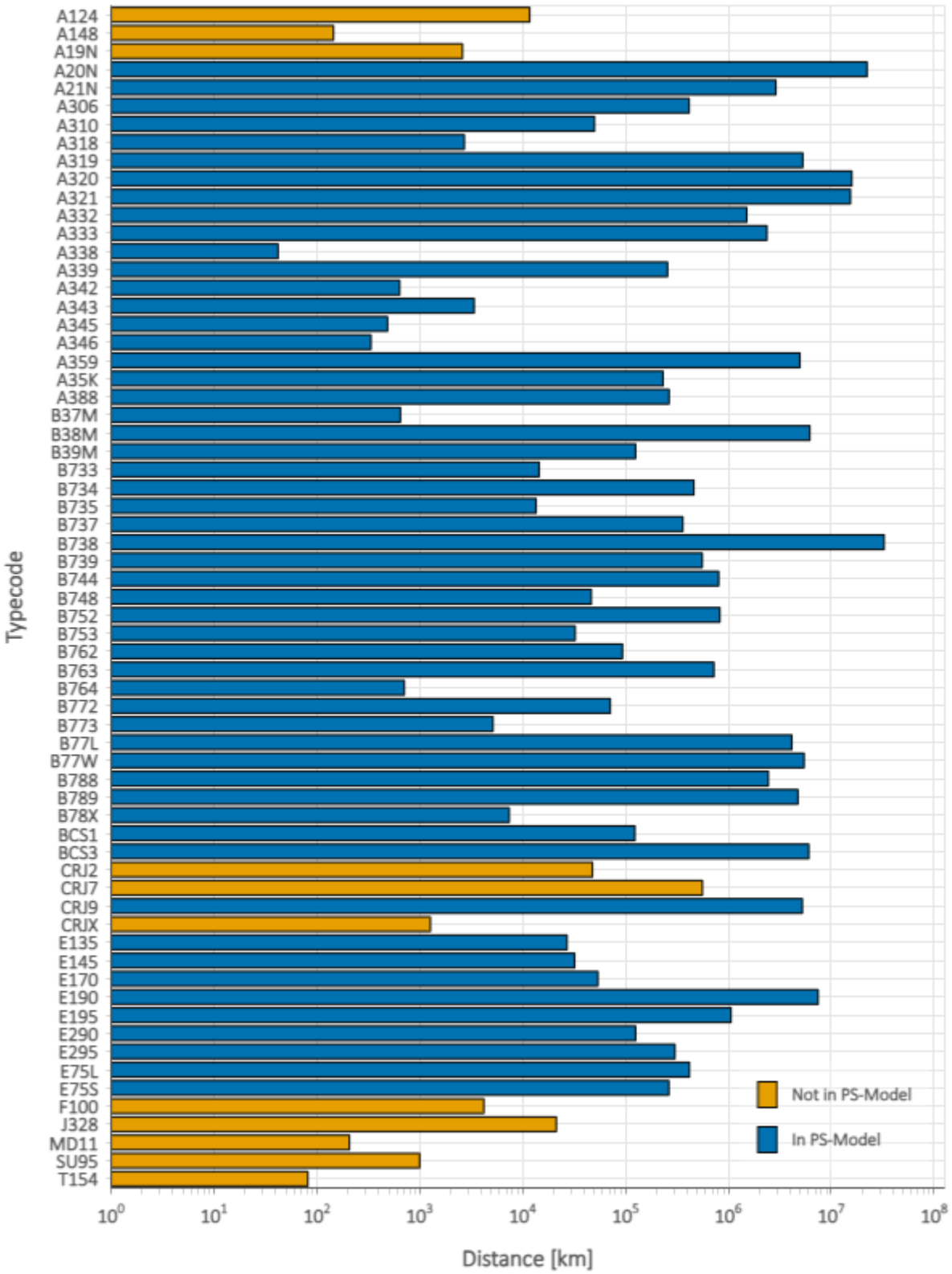

Figure 6: Distance flown per typecode in the studied dataset, with a logarithmic x-axis.

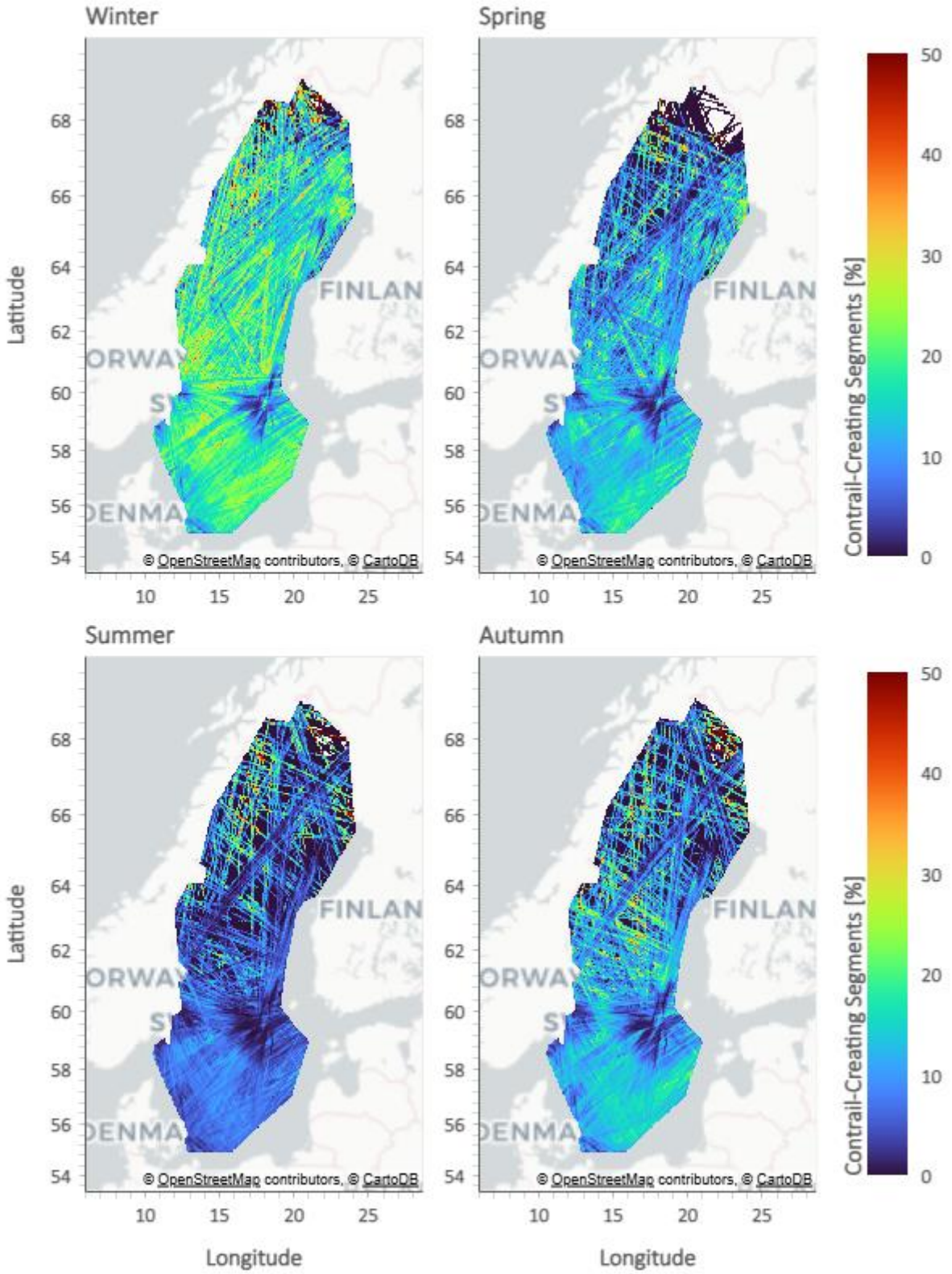

Figure 7: The lateral percentage of contrail formation according to the CoCiP model, per season.

The vertical distribution of contrail formation, as modelled with CoCiP, can be seen in *Figure* 8. Because this is based on historical data, it shows where contrails were modelled to have been formed, influenced by the distribution of all flight segments, and not necessarily where they are most likely to form. It does however show that contrails only formed between 19 750 and 43 000 feet, with half of the contrails concentrated between 34 000 and 37 000 feet. Cooling contrails appear more concentrated with a median near 36 000 feet, while warming contrails are slightly less concentrated with a median near 35 500 feet. Again, this is based on data from actual flights and is thus influenced by which altitudes aircraft typically fly at. The distribution of EF per altitude and season is shown in *Figure 9*, illustrating how altitude and season also affect the magnitude of resulting EF. This shows that the altitude contributes to a difference in the results between the spring and autumn seasons according to the CoCiP model. While contrails can form in a larger range of altitudes in winter than in summer, this difference also appears true for spring in comparison to autumn, which otherwise produce similar results to each other.

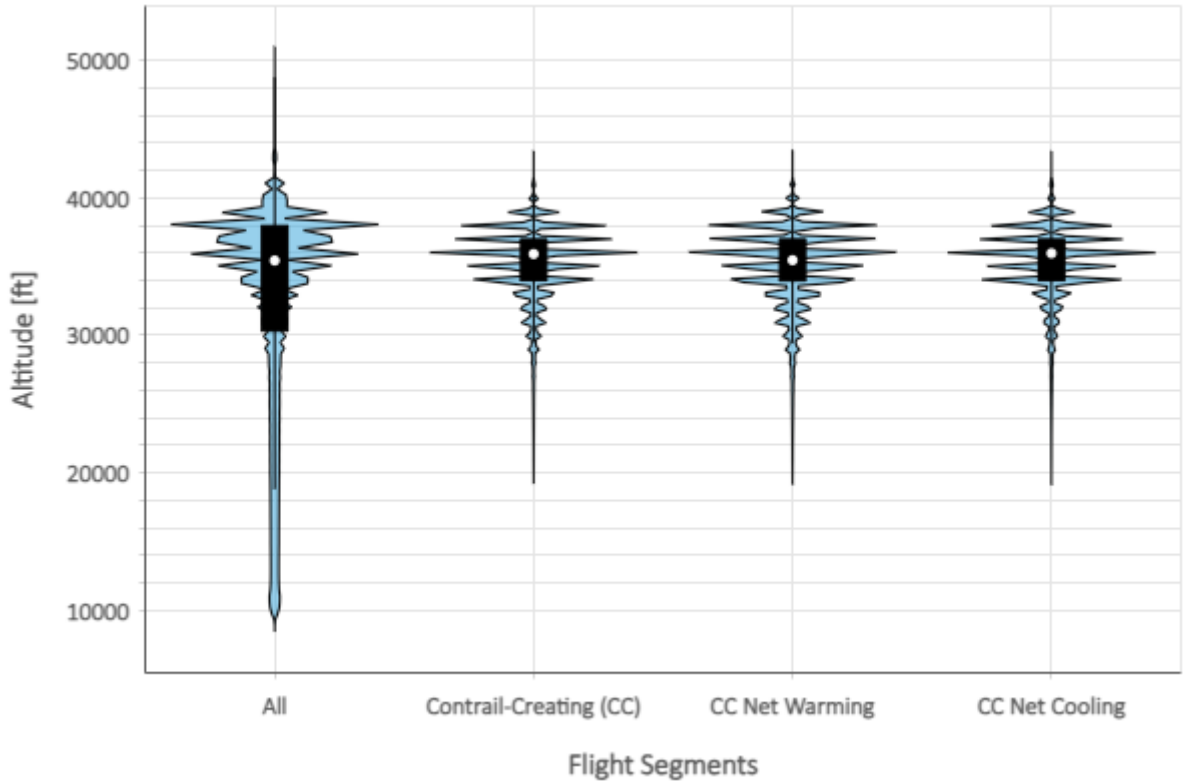

Figure 8: The vertical distribution of the dataset and resulting contrail-creating segments from the CoCiP model.

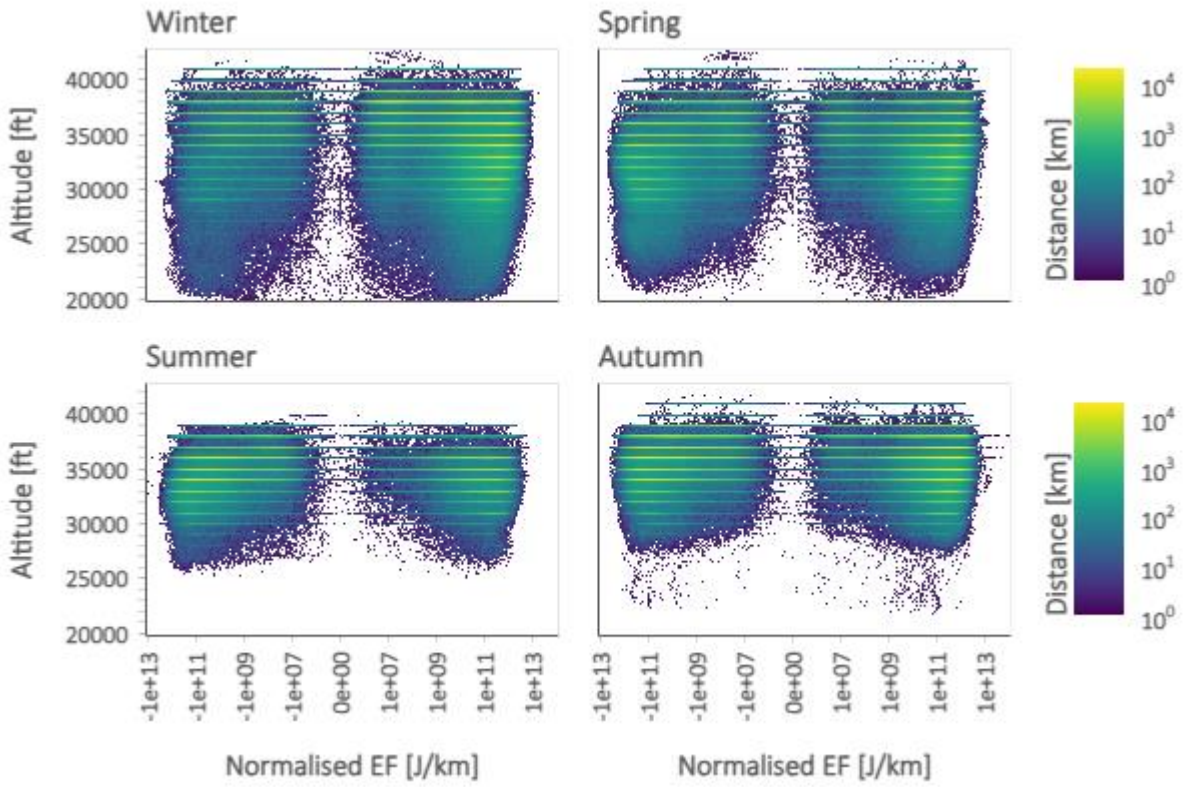

Figure 9: The vertical distribution of EF from the CoCiP model, per season.

Figure 10 and *Figure* 12 show the average EF per altitude and latitude, and per altitude and longitude, respectively, for both the contrail aCCF and CoCiP. The percentage distributions of contrail formation for the same domains are shown in *Figure 11* and *Figure* 13, in comparison with *Figure 5* of total traffic. These show a high discrepancy between the number of contrails that form according to the contrail aCCF and the CoCiP model. They do, however, display similar dependencies at which altitudes contrails can form per season. While warming contrails dominate the winter, spring and autumn seasons, cooling contrails appear to have a near-equal impact in the summer. There also appears to be a latitudinal trend where the range where contrails are most likely to form shifts towards slightly lower altitudes with an increase in latitude. This also shows among the easternmost longitudes which only have data points from the northern latitudes, otherwise it is difficult to identify any longitudinal dependency.

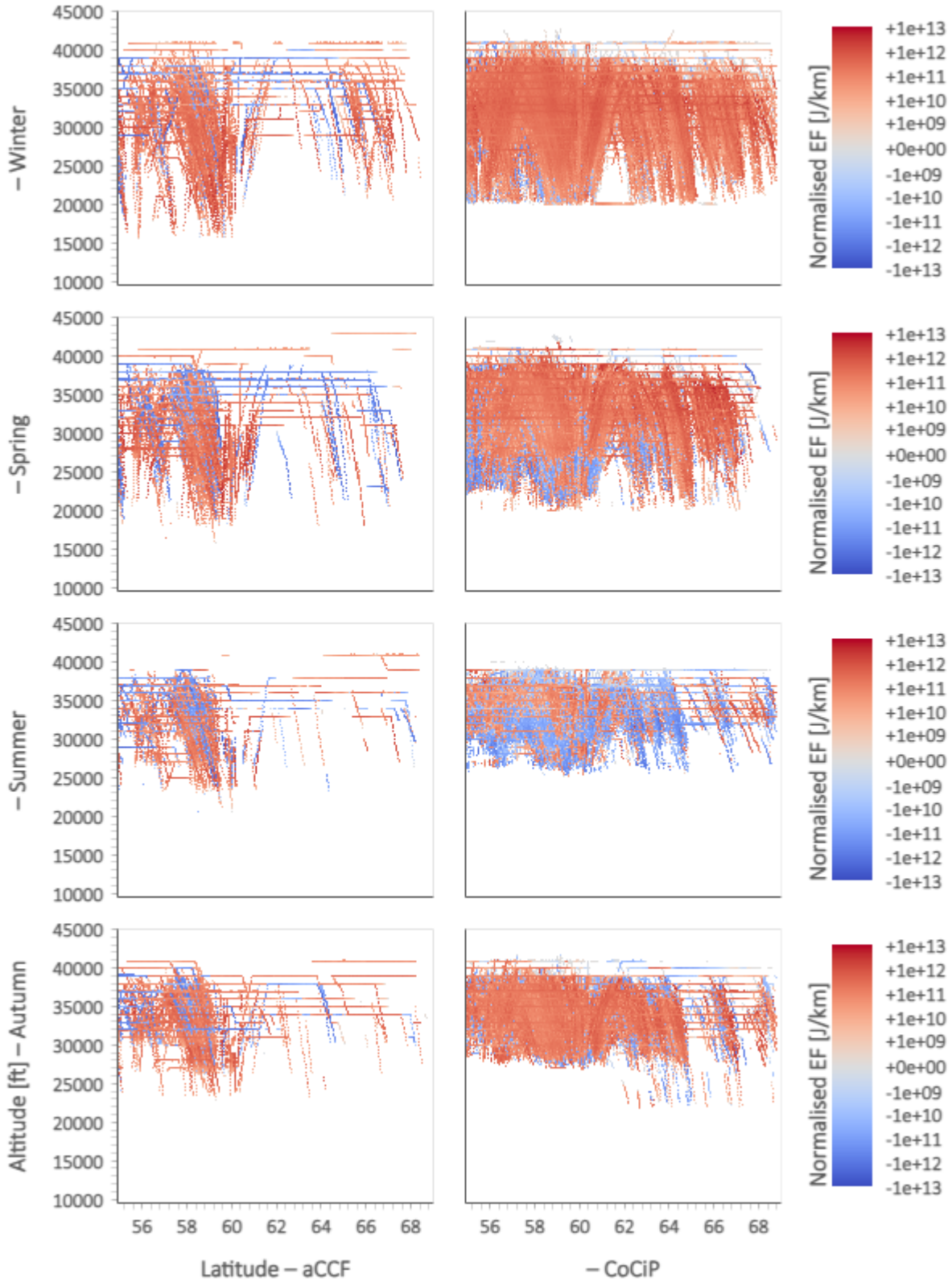

Figure 10: The normalised EF per latitude and altitude for the aCCF and CoCiP.

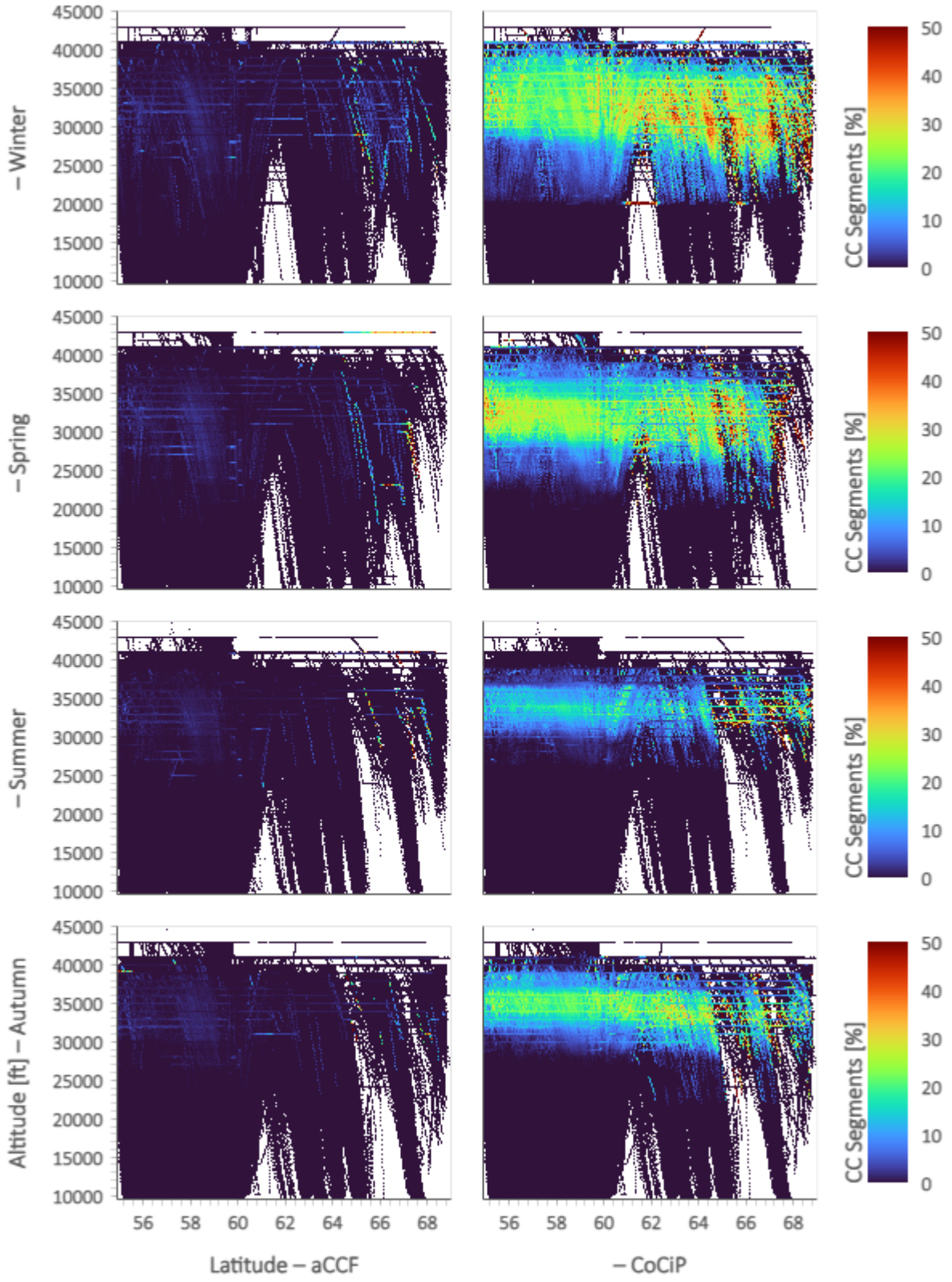

Figure 11: The percentage of contrail forming segments per latitude and altitude for the aCCF and CoCiP.

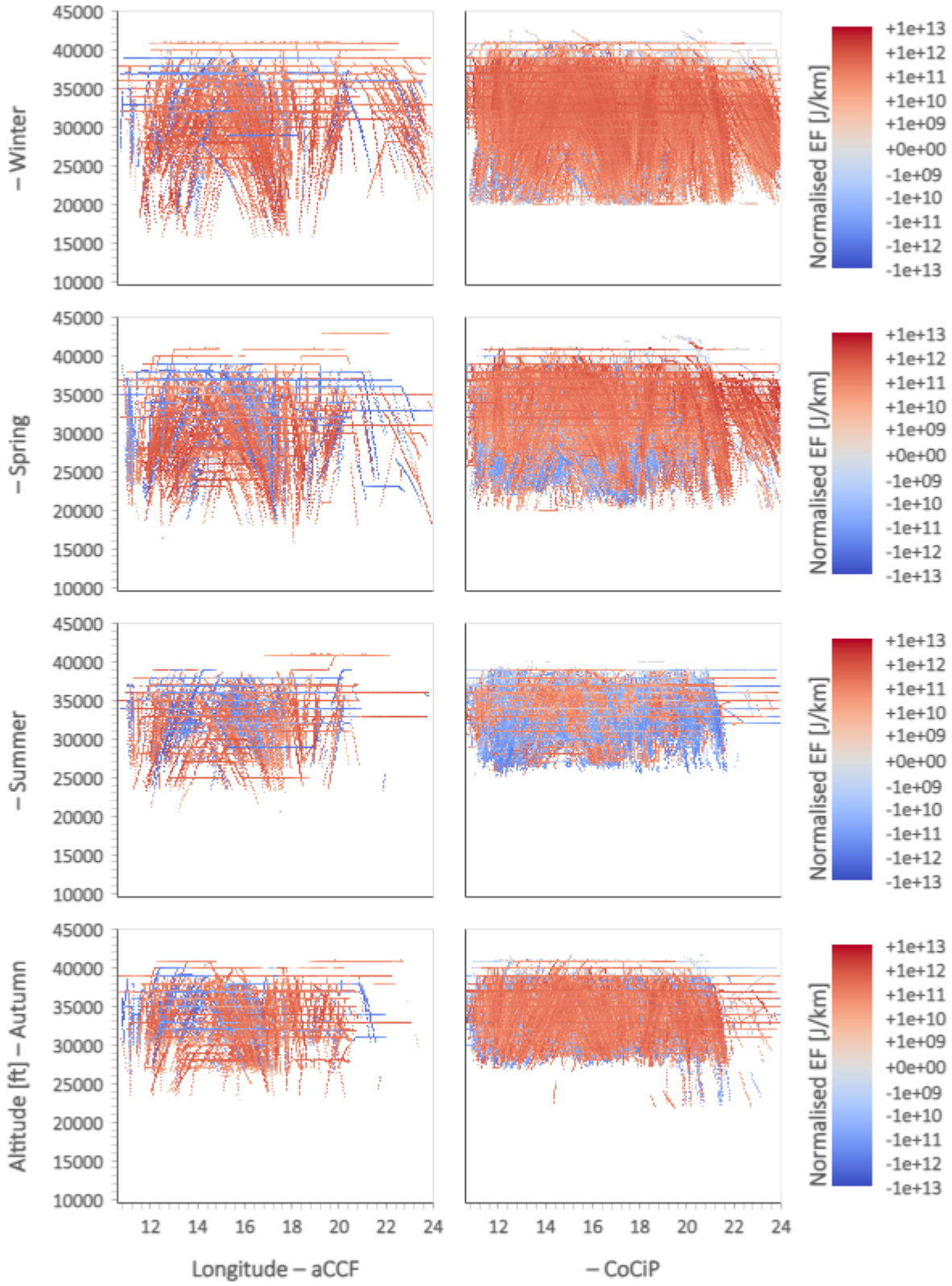

Figure 12: The normalised EF per longitude and altitude for the aCCF and CoCiP.

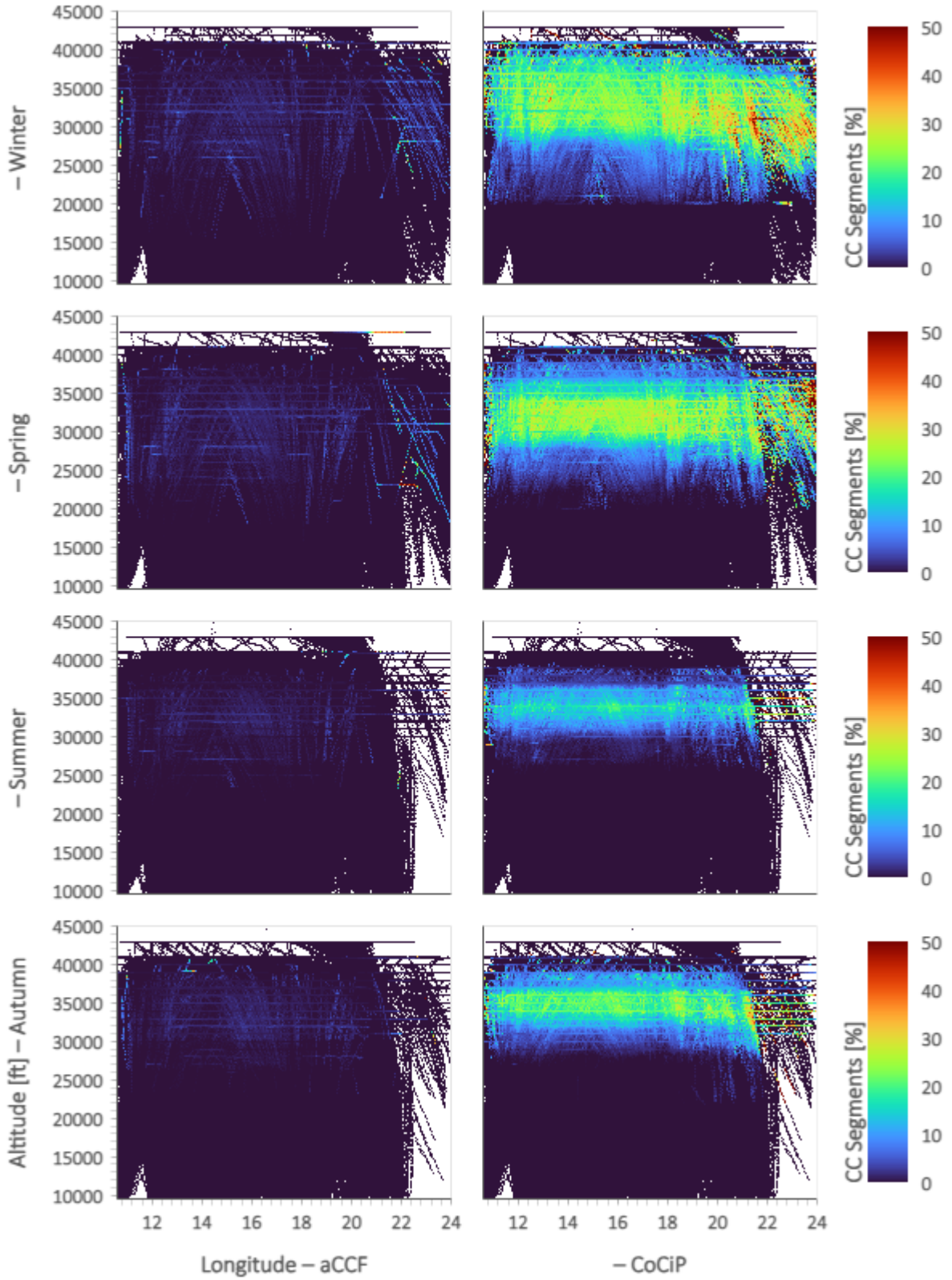

Figure 13: The percentage of contrail forming segments per longitude and altitude for the aCCF and CoCiP.

The difference in EF as modelled by the contrail aCCF and CoCiP is shown per season in *Figure 14*. Segments where both models form no contrails are excluded. Ideally, these plots would show a 1:1 proportional relationship, instead, they show large discrepancies for all seasons. The lines at zero on either axis indicate that contrails formed according to only one of the models. The CoCiP model gives flight segments with EF that span six orders of magnitude, while the aCCF only spans two orders of magnitude. When contrails are formed according to both models, they typically agree on whether they are warming or cooling. However, there are also several segments with the opposite result.

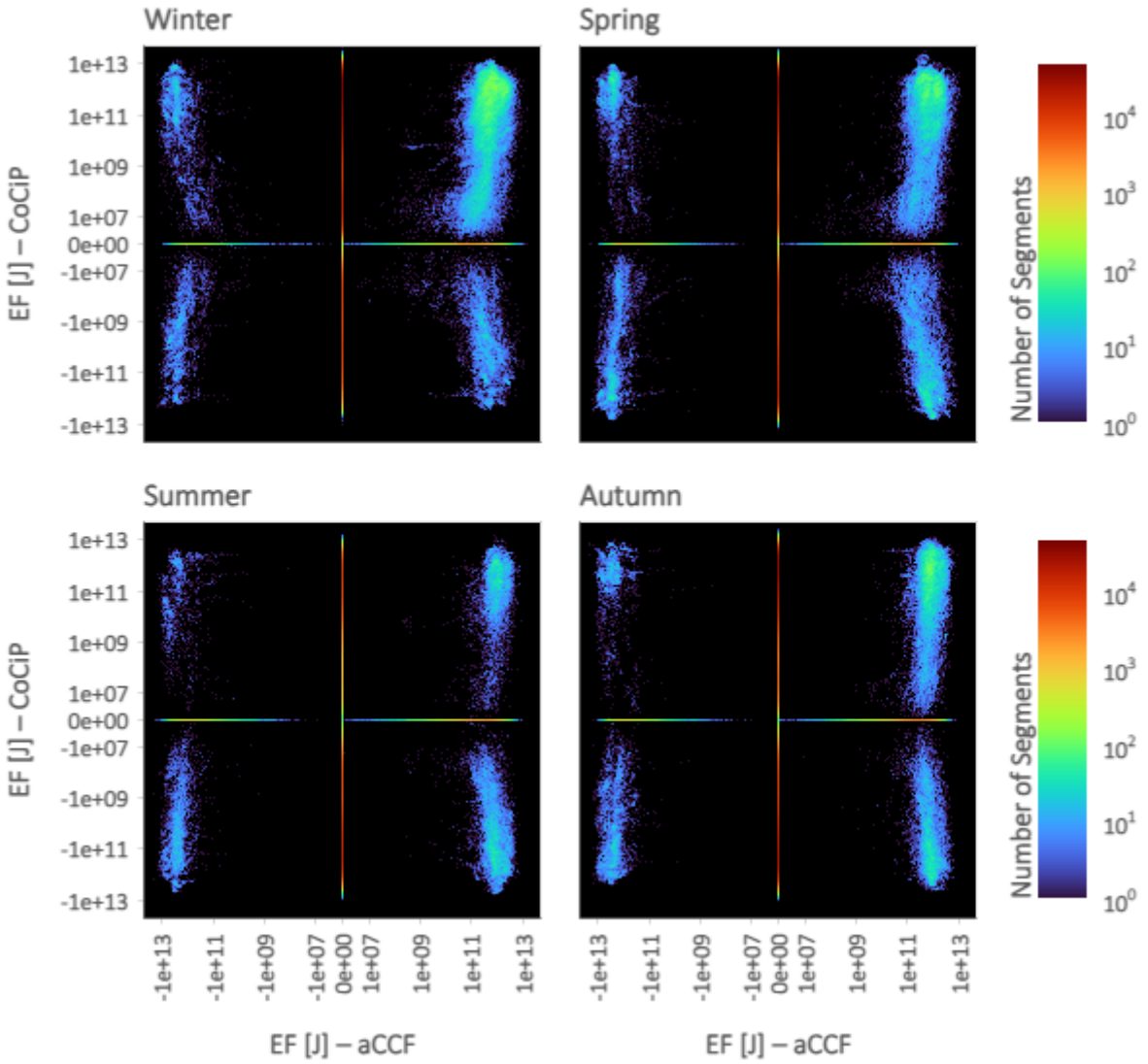

Figure 14: Comparison of EF as modelled by the aCCF and CoCiP, per season.

For the time-of-day dimension, *Figure 15* shows that warming contrails dominate during the afternoon, while cooling contrails form mainly during the day. While cooling contrails are more common than warming ones in the summer, the autumn appears to have more of them in absolute numbers. Cooling contrails also appear more common than warming ones in the morning in spring and autumn. For comparison, *Figure 16* shows the EF per contrail segment, i.e. with the effect of the contrails over their lifetime rather than for the time of formation. As expected, when the results from the contrail segments are aggregated back to the flight segments, the warming effect from the evening in the latter figure appears earlier in the afternoon in the former. In addition, *Figure 17* displays the mean and median EF. The difference between the mean and median is in agreement with findings that contrails from a limited set of flights account for most of the contribution of EF.

The net total EF from the contrail aCCF and CoCiP is presented in *Figure 18* along with the P-ATR20-based fuel burn results converted to EF for the contrail-forming segments from both respective models and for all segments in the studied dataset. The EF results from contrails modelled by CoCiP have a larger effect than the total fuel consumption from all studied trajectories by an order of magnitude for winter, spring and autumn. The only season in which the net total EF is lower is the summer. Both models produce a higher net total contribution from contrails than the fuel consumption from the contrail-forming flight segments, for all seasons.

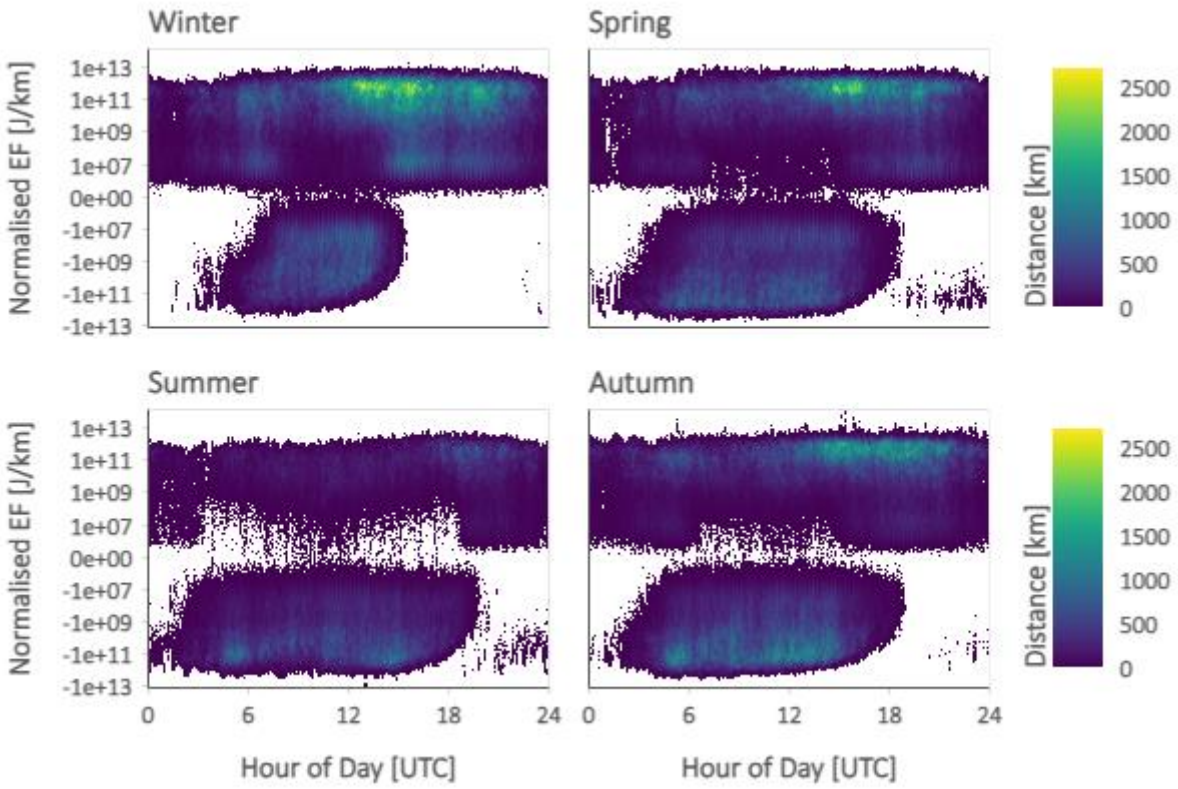

Figure 15: Distribution of EF depending on time of day at contrail formation by the CoCiP model, per season.

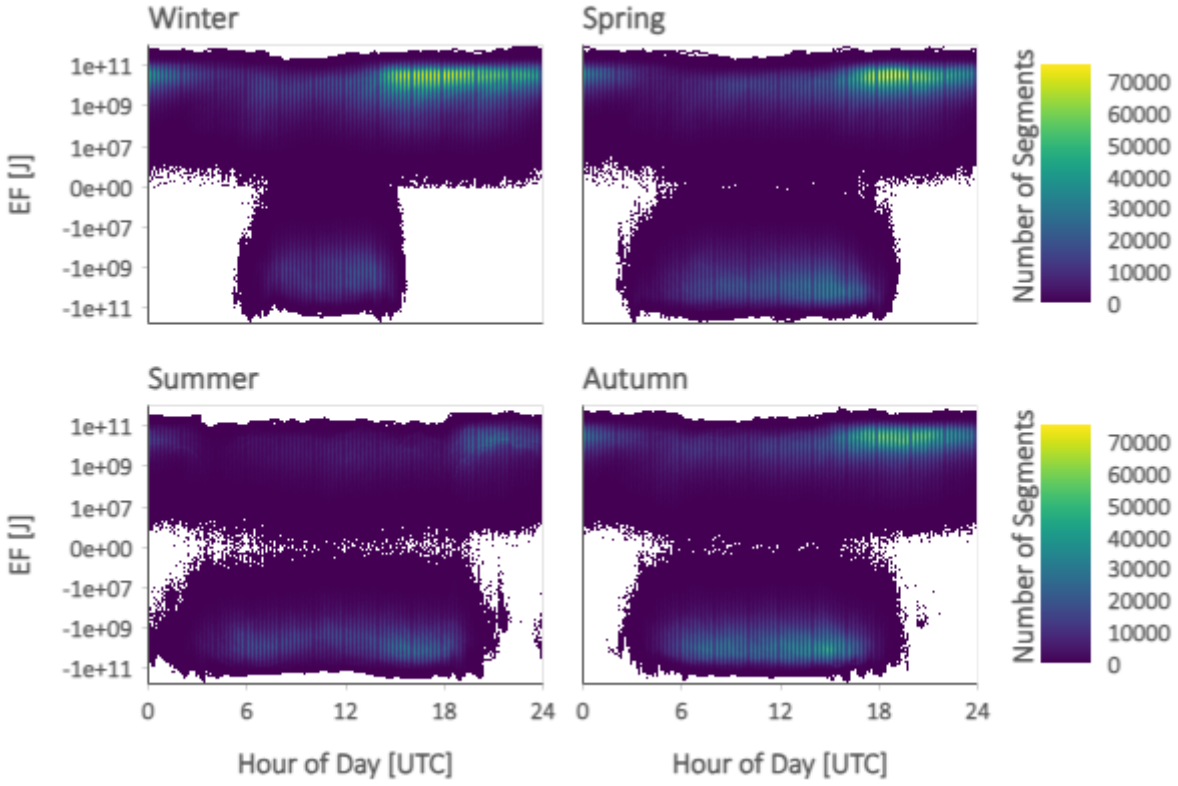

Figure 16: Distribution of EF depending on time of day by the CoCiP model, per season.
The time integration per contrail segment is 300 s for segments initially formed under 10 s.

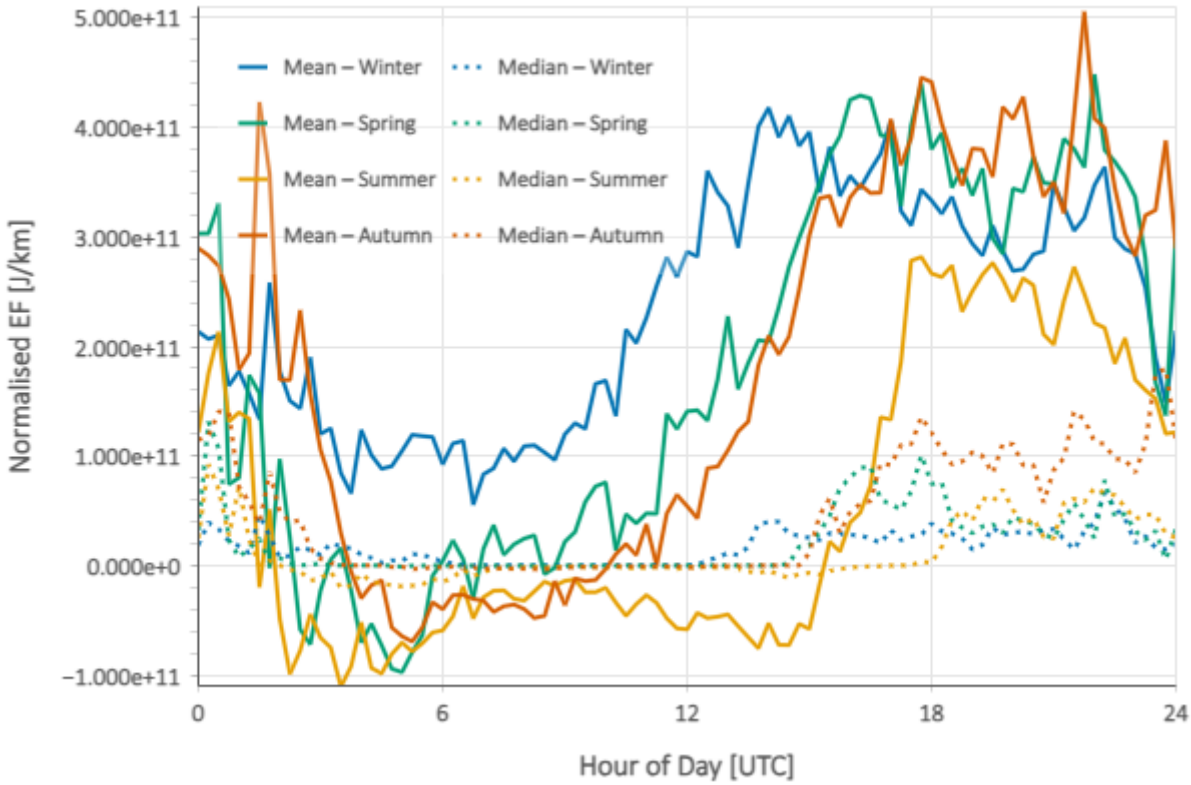

Figure 17: Mean and median EF depending on time of day at contrail formation by the CoCiP model, per season.

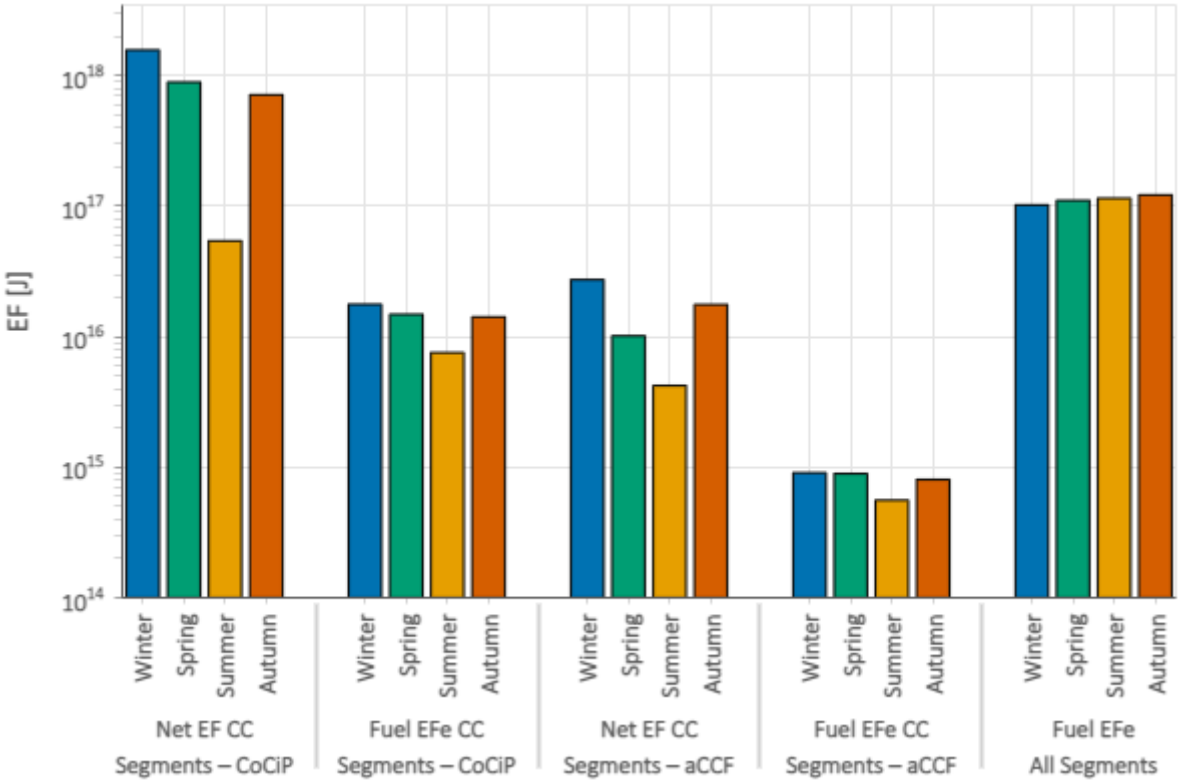

Figure 18: The net total EF from contrail-creating (CC) segments, and the EF equivalents (EFe) from the fuel burn.

7.3. Contrails per Aircraft Typecode

Results per typecode are presented for the 16 most common typecodes in *Figure 6* as modelled with CoCiP and the PS-model, which includes widebodies and narrowbodies from two generations of aircraft and two regional airliners. *Figure 19* shows the net total EF per typecode and season, *Figure 20* displays the distance flown and percentage of contrail formation per typecode, and *Figure 21* illustrates the normalised EF per distance. These results show that, within Swedish airspace, short- to medium-haul aircraft are the greatest contributors to total EF, mainly due to the significantly longer distance covered by these aircraft. In the normalised results, the A21N, B38M, and B788 and B789 show lower EF compared with the A321, B738, and B77L and B77W, respectively, despite not differing to the same extent in the percentage of segments where contrails are formed, suggesting that aircraft of the newer generation are less likely to produce persistent contrails. However, the A333 and A359 produce similar results to each other, and the opposite pattern is observed for the A20N in comparison with the A320. Again, this may be influenced by the fact that the engine type and mass are unknown in this dataset, and potentially also by traffic patterns.

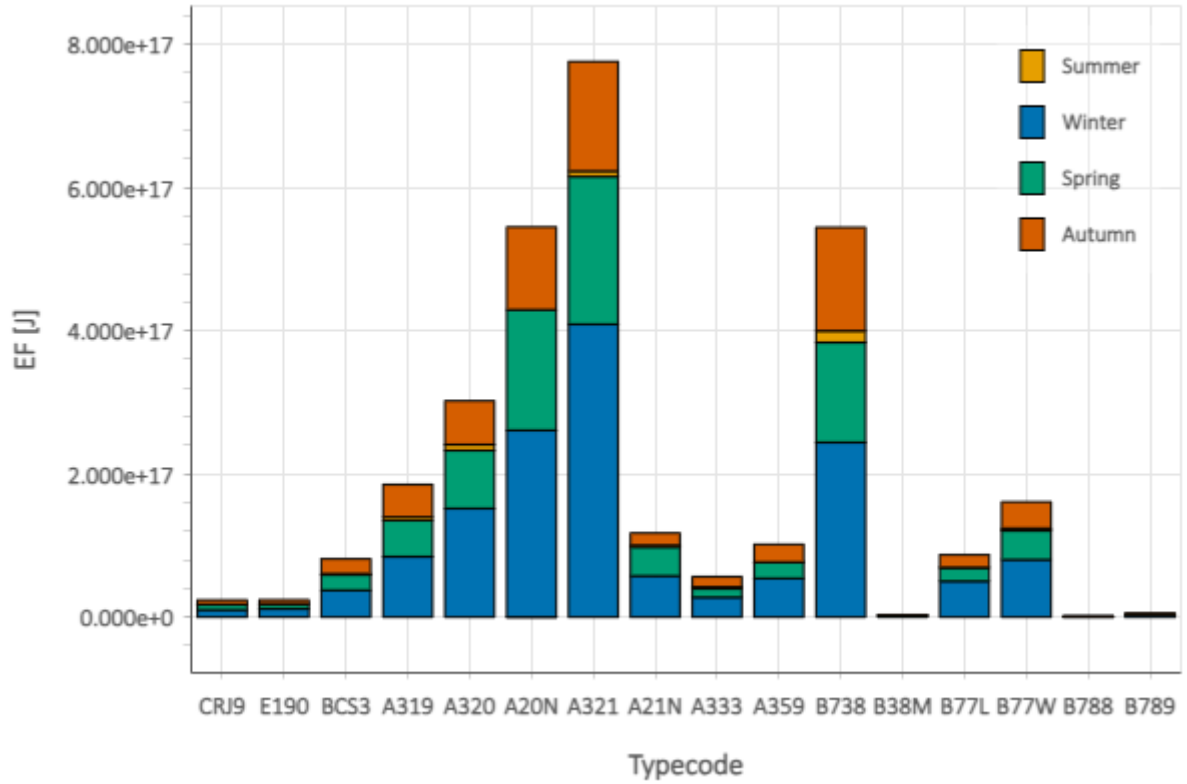

Figure 19: The net total EF from the sixteen most common aircraft typecodes, per season.

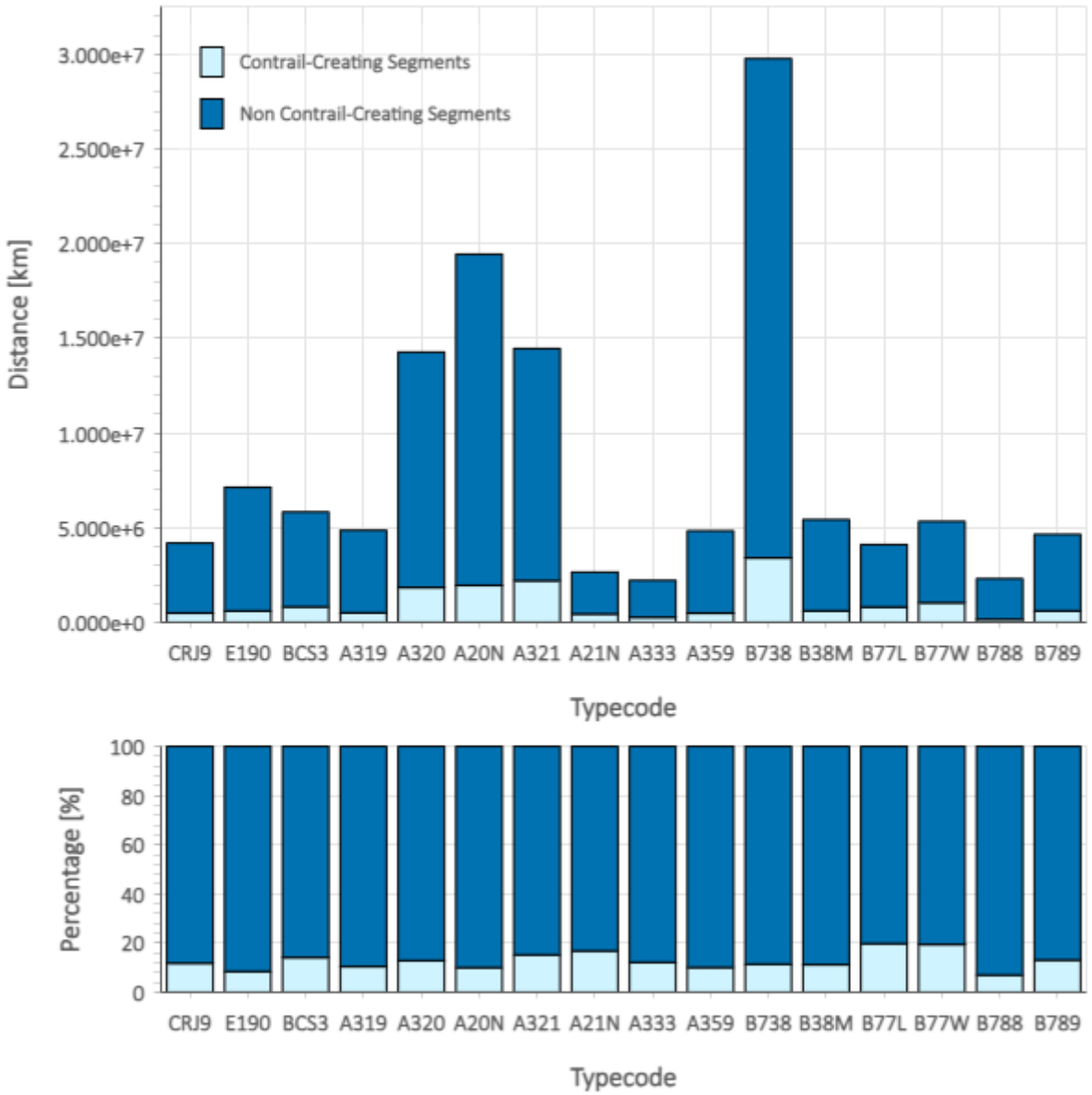

Figure 20: Distance flown and percentage per typecode above 19 750 feet, classified after whether contrails were formed.

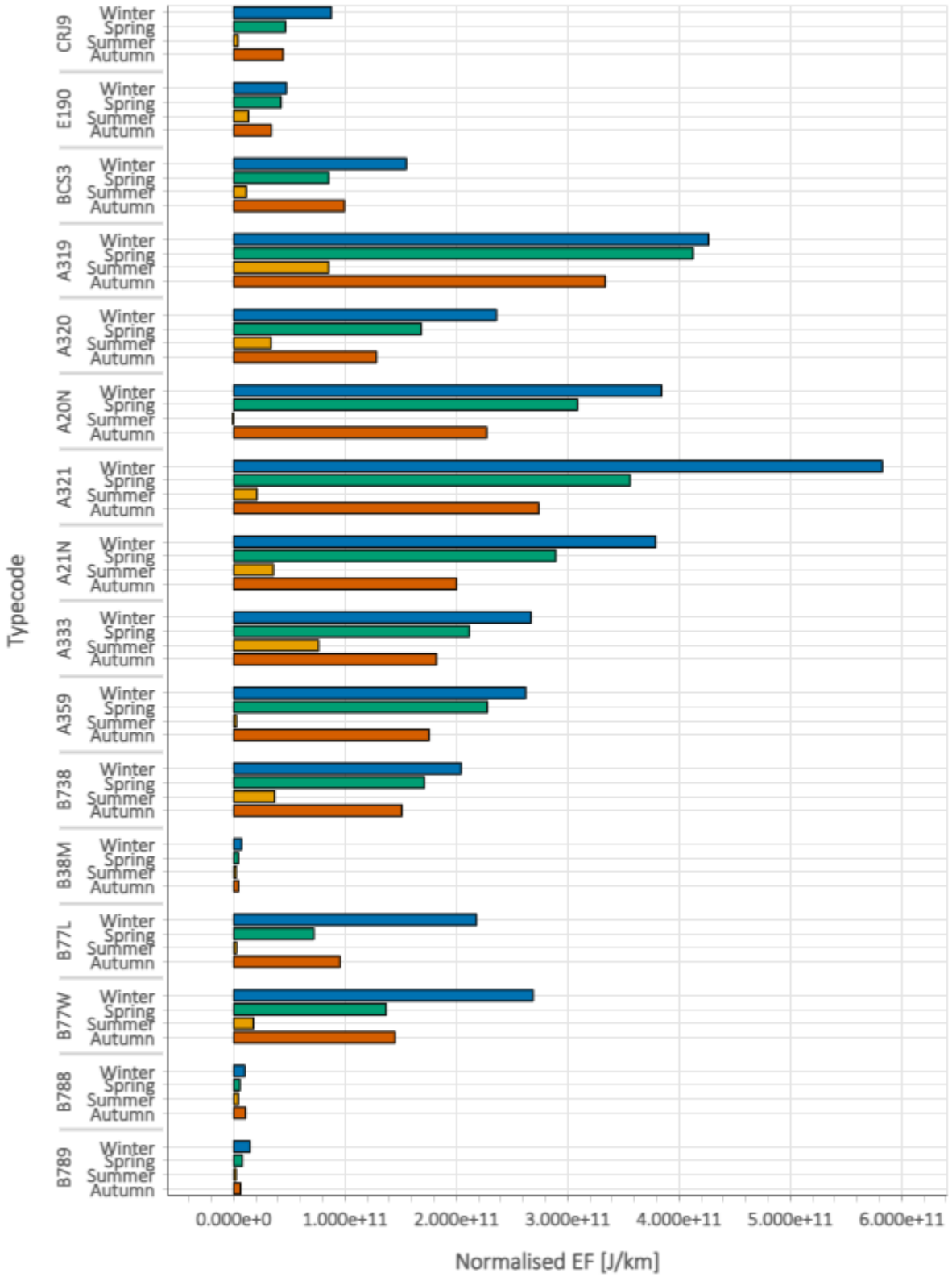

Figure 21: The normalised EF for the sixteen most common typecodes, per season.

Figure 22 shows the same comparison between the contrail aCCF and CoCiP as *Figure 14* with similar results, but now for the 16 most common typecodes instead of per season.

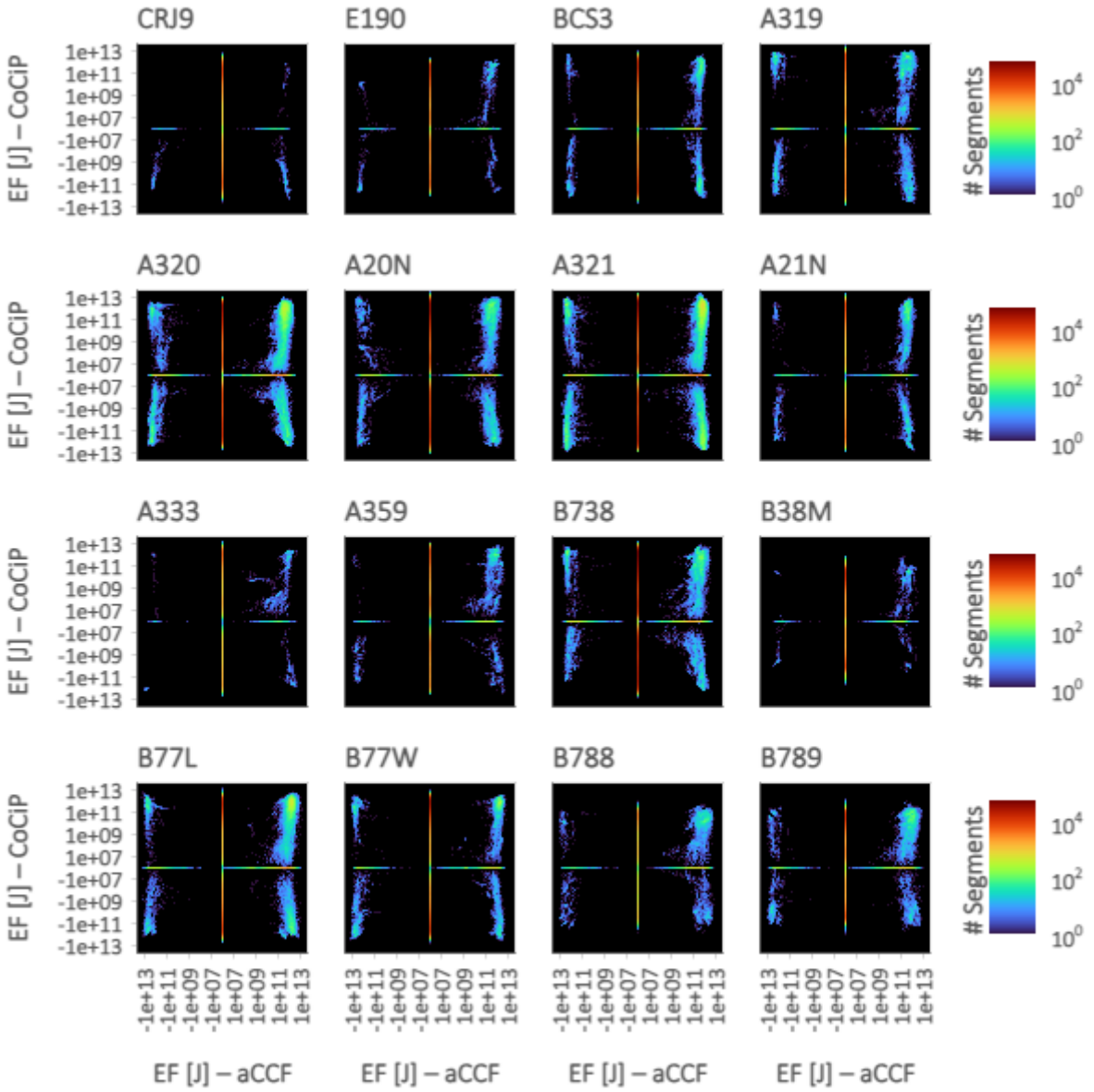

Figure 22: Comparison between the contrail aCCF and CoCiP results, for the 16 most common typecodes.

7.4. Optimisation Results

The optimisation results are divided into two categories: full flights including a climb, cruise, and descent phase, and overflights including waypoints above 20 000 feet only. The net total EF from the original flights compared with their optimised trajectories is shown for both categories and per season in *Figure 23*. In the square plots, the lower-right triangles indicate an improvement. This is where most data points are found. However, some overflights see an increase in EF after the optimisation. For full flights, the typical result is that contrail formation is avoided altogether, i.e. where the EF for the optimised trajectory is 0. This also occurs for trajectories in both categories that initially formed cooling contrails. It also shows that a slightly cooling overflight may become several orders of magnitude more cooling. A significantly warming flight may also become significantly cooling, and vice versa.

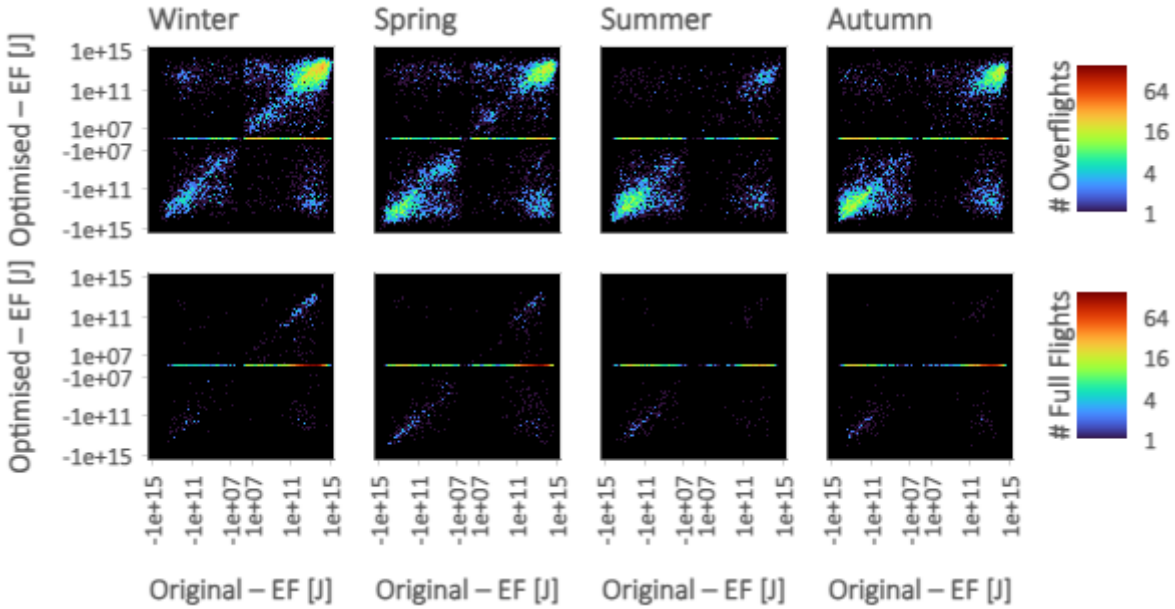

Figure 23: Comparison of the modelled EF between the original and optimised trajectories.

The resulting vertical trajectories for overflights are presented per season in *Figure 24*, alongside the original trajectories and their differences. The equivalent results for full flights are shown in *Figure 25*. While some overflights ascend to higher altitudes, many descend by several thousand feet with the current setup of the trajectory optimiser model, including descents below an altitude of 20 000 feet where the lowest contrails form. For full flights, the optimisation model generally favours level flight at lower altitudes, although a few optimised trajectories occur at higher altitudes than the original ones.

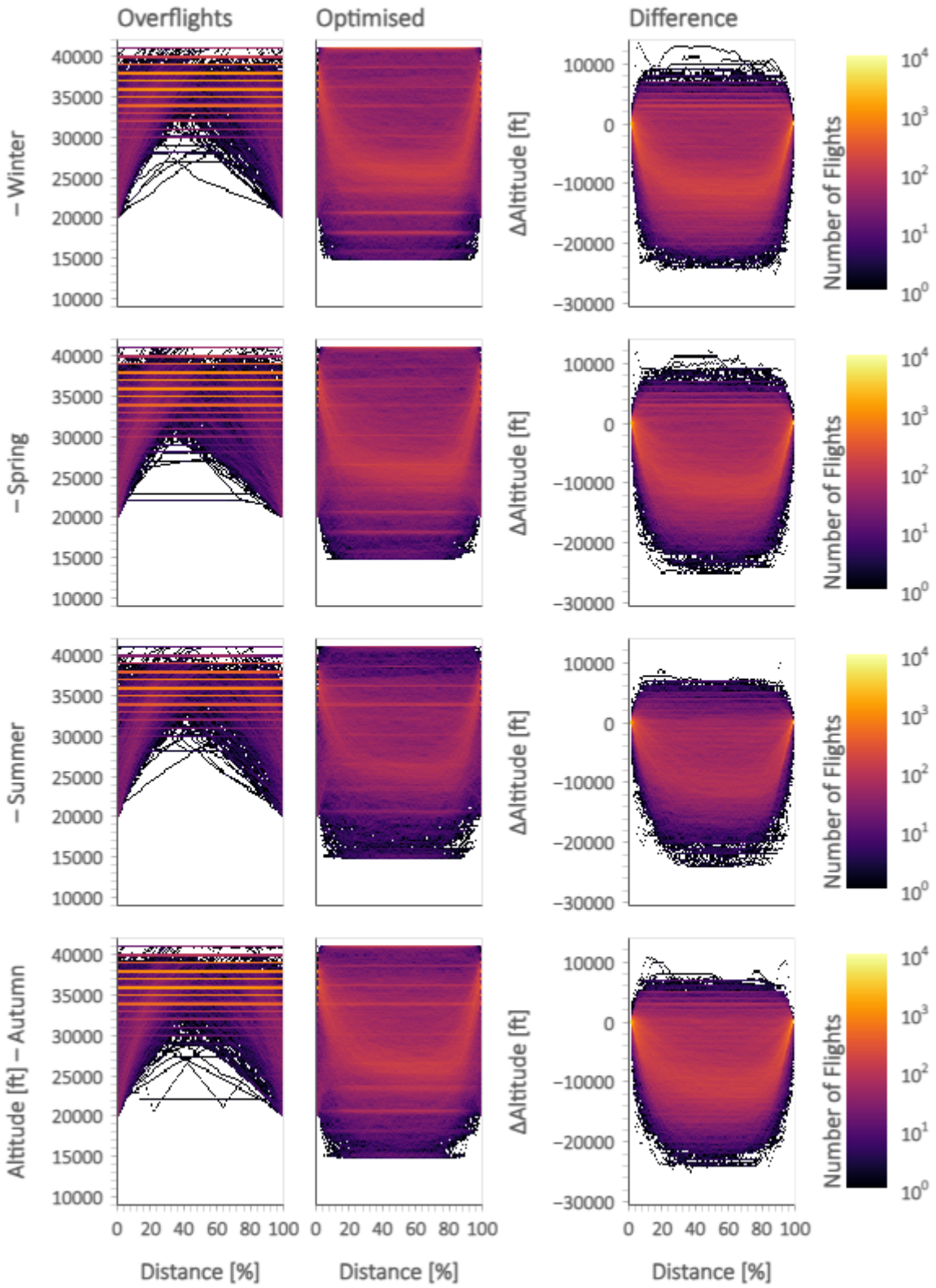

Figure 24: The original and optimised trajectories of overflights, including the difference between them, per season.

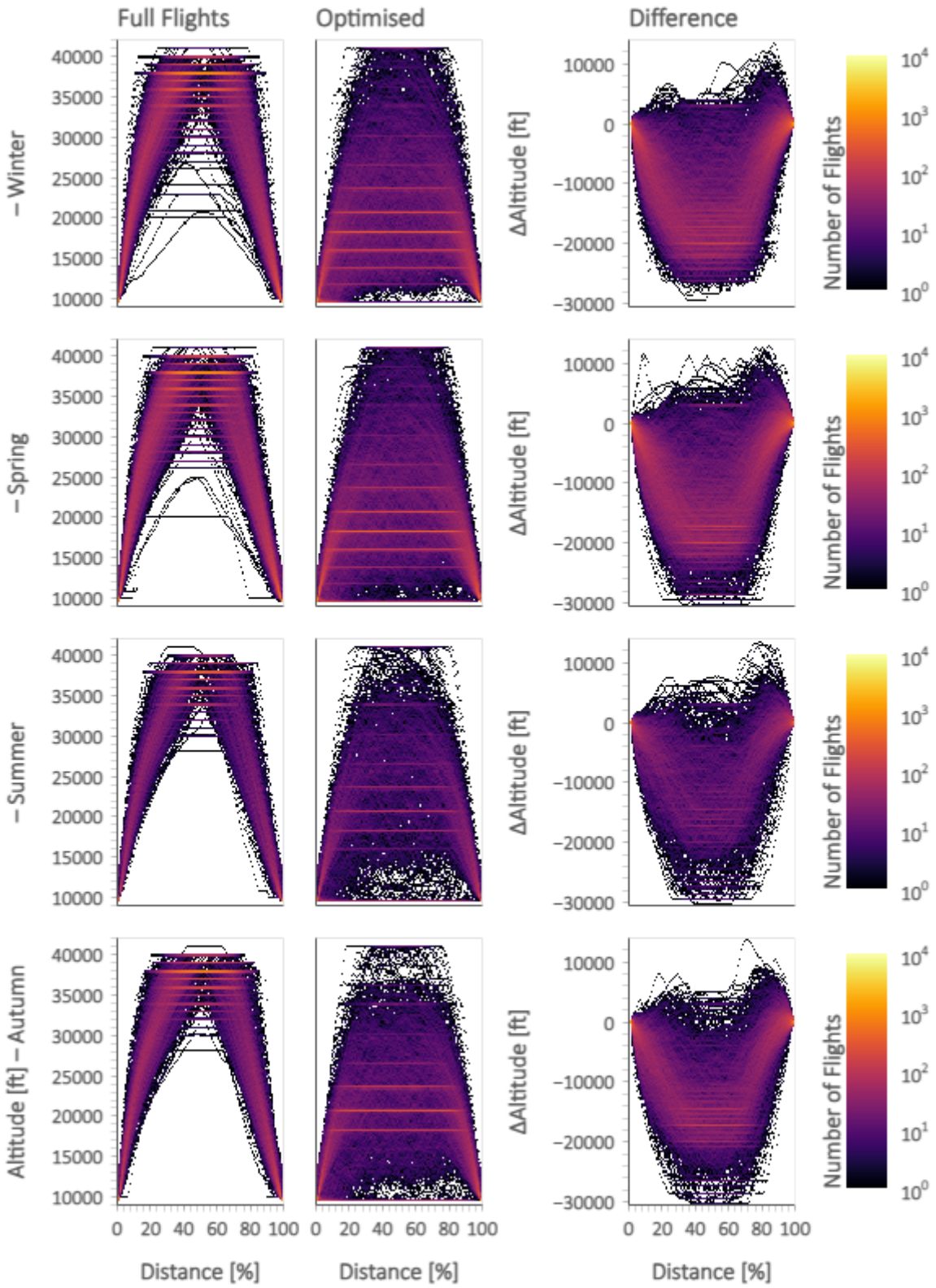

Figure 25: The original and optimised trajectories of full flights, including the difference between them, per season.

To assess whether improvements of EF come with an increased fuel burn, the difference in EF per flight is plotted against the difference in fuel burn in *Figure 27*. Results appear in all quadrants, and therefore the difference in EF and fuel burn are both also plotted against the difference in time in *Figure 28* and *Figure* 29, respectively. While the time was constrained to 1.10 of the original trajectories to allow for extra time for altitude changes, it is noticed that a large part of the optimised trajectories hit this constraint, presumably due to a lower resulting fuel burn. A few trajectories see a decrease in both EF and fuel burn; however, most see a decrease in EF and an increase in fuel burn. It is unexpected to see trajectories with both a decrease in time and in fuel burn, including some overflights with extreme values. Several overflights also breached the time constraint, even if it is seen that it became an active constraint for others. Therefore, the flights in the grey fields of *Figure 26* and *Figure* 29 have been omitted from the other optimisation results.

The optimisation results are also presented per typecode in *Figure 26*. This shows whether the optimisation led to an improvement or worsening of the net total EF for the flight. The empty bars indicate that no flight existed for that category–typecode combination. The black fields are where the optimiser failed to converge on a feasible solution, and the grey fields show the proportion of the cleaned and omitted data indicated in *Figure 29*.

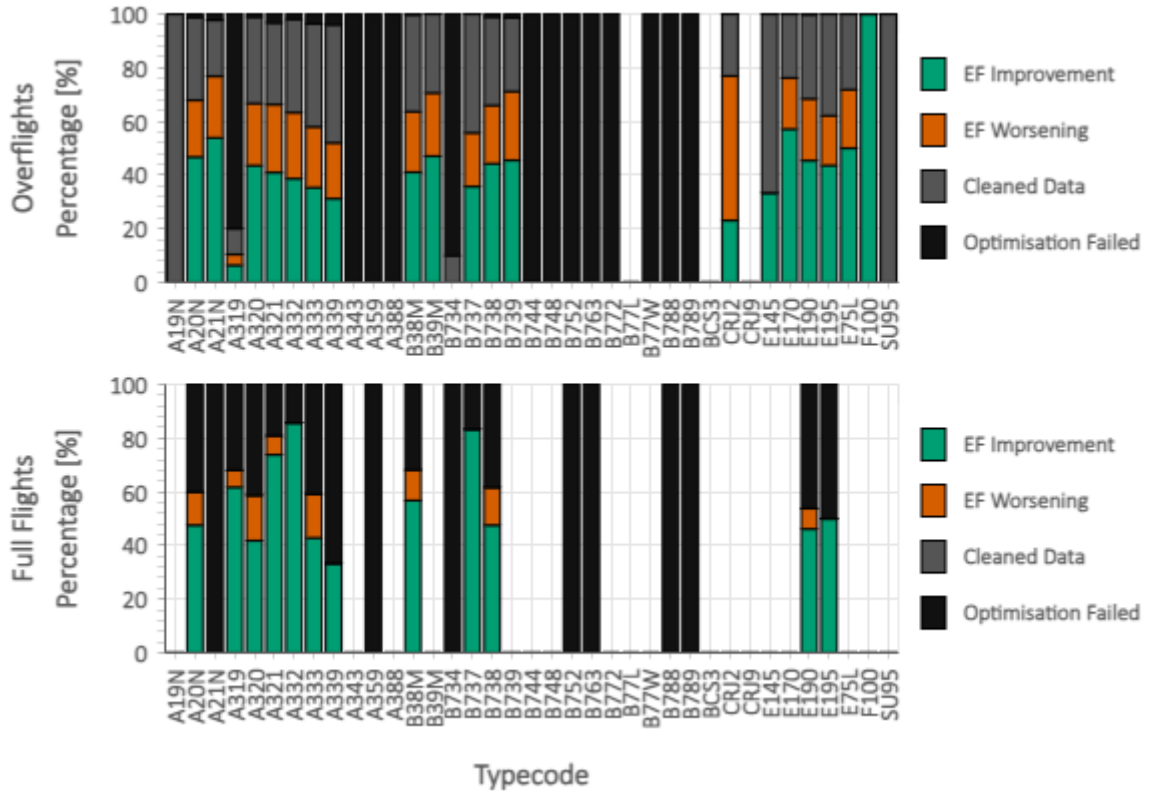

Figure 26: The general results from the optimisation per flight category and typecode.

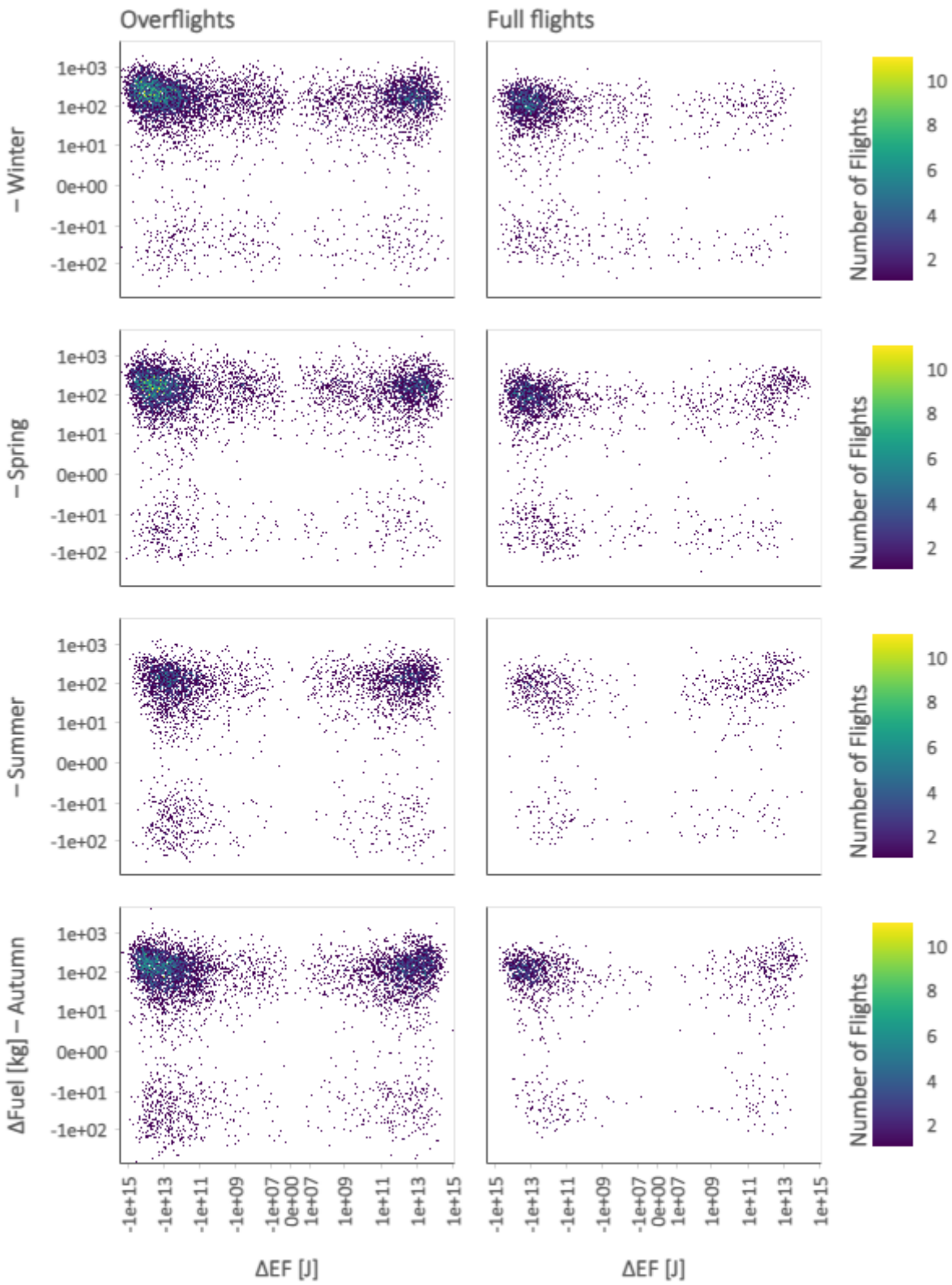

Figure 27: The difference in EF and fuel burn for both optimised overflights and full flights, per season.

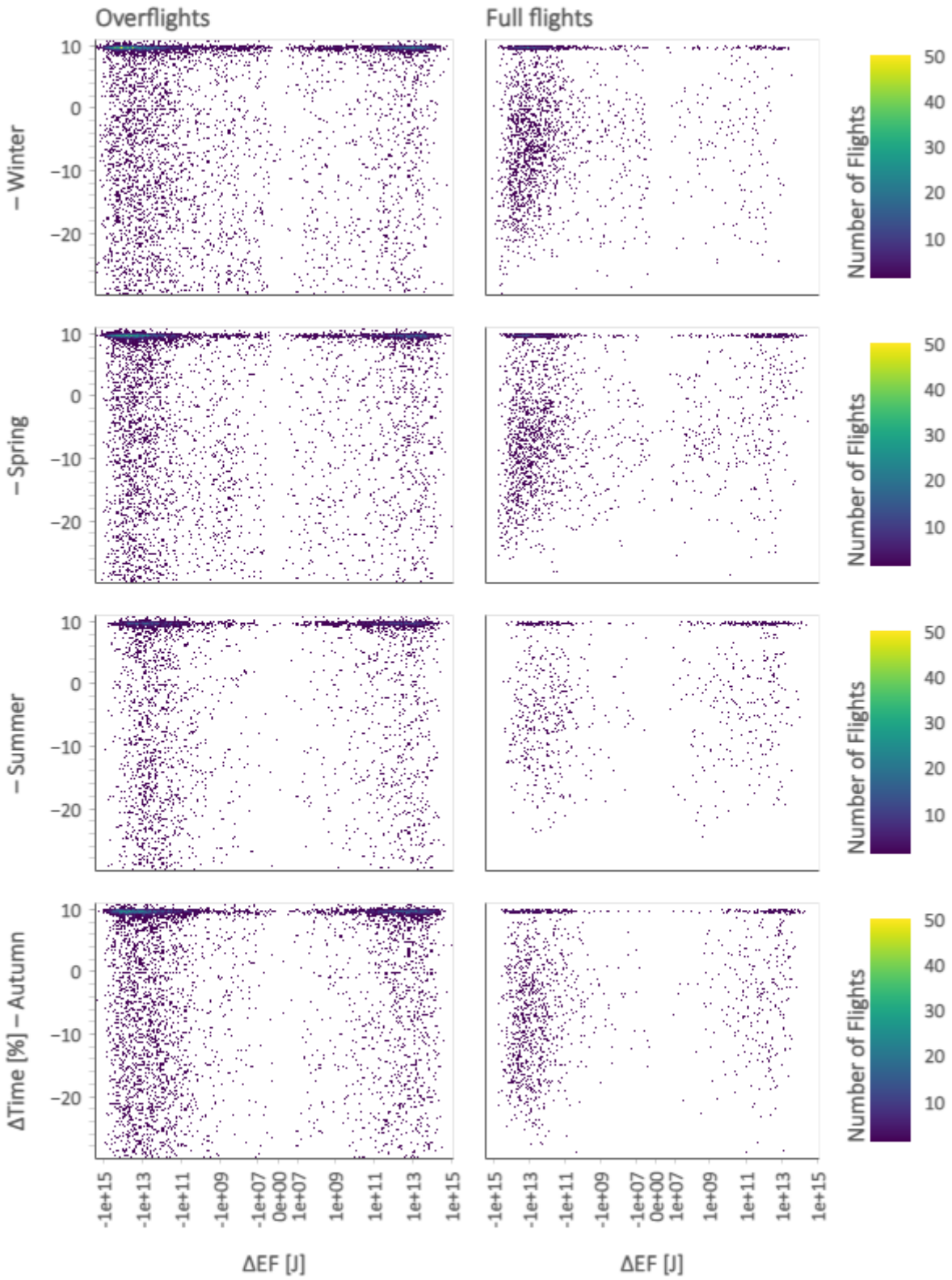

Figure 28: The difference in EF and time for both optimised overflights and full flights, per season.

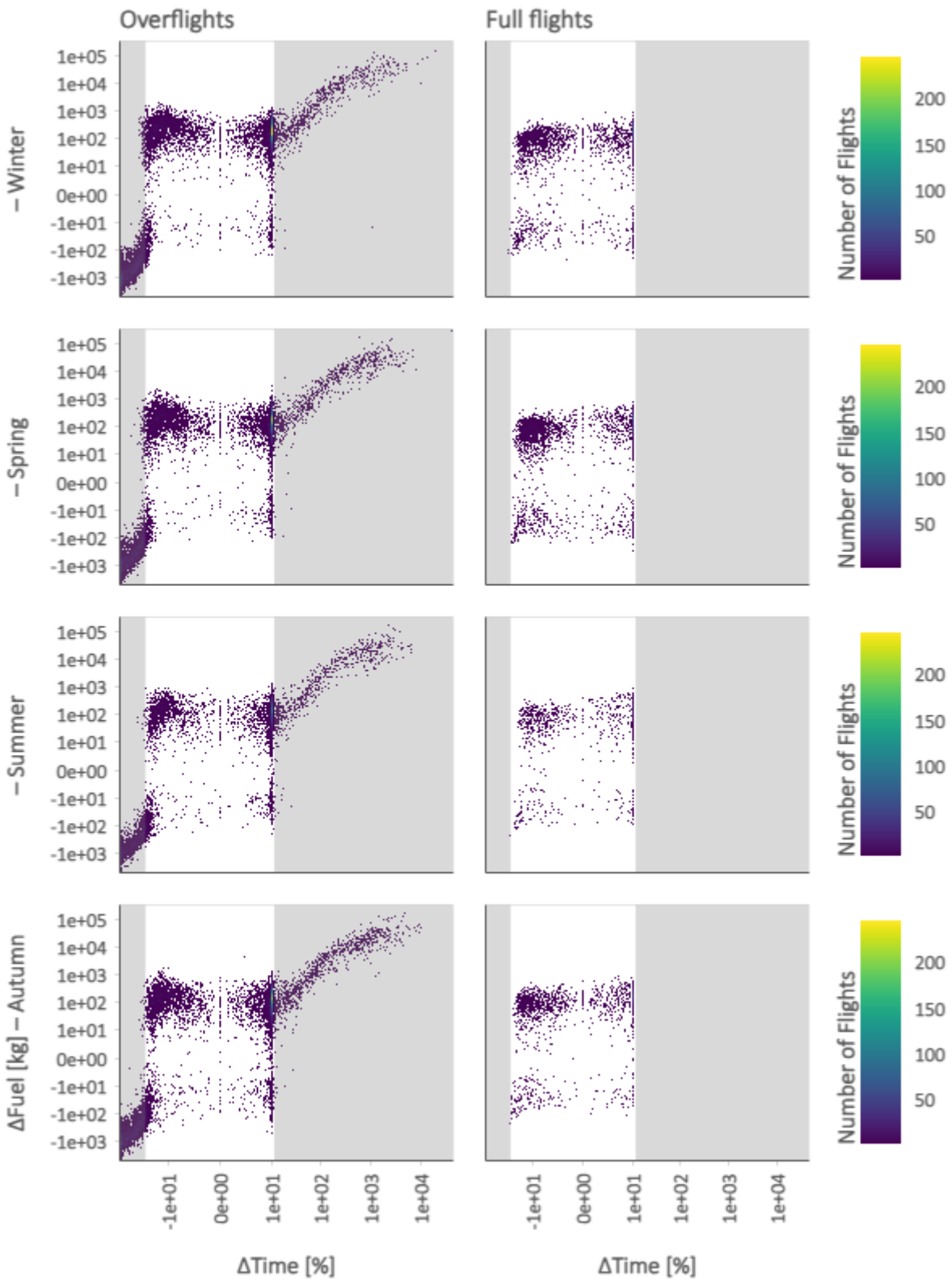

Figure 29: The difference in time and fuel burn for both optimised overflights and full flights, per season.

8. Discussion

The discussion section follows a path over the major sections of this work. It takes off from the reasoning behind the choice of data sources and thereafter continues with an evaluation of the models and methodological choices. The discussion then follows with the interpretation of the results and onto considerations of how these findings relate to other mitigation strategies, before landing at future research opportunities.

The ECMWF ERA5 is a common source for historical meteorological data in related works within a European context, and its drawbacks have led to the works brought up in *Section 4.3.1* related to the correction of humidity data. As previously noted by other researchers, the real challenge is to collect sufficient real-time data on meteorological conditions at cruising altitudes to be able to create reliable forecasts suitable for flight planning, but potentially also for real-time mitigation. This would require the installation of sufficiently accurate humidity sensors on aircraft on a much larger scale than the specially equipped aircraft in the last decades. The meteorological data should also be transmitted by the aircraft such that others can benefit from it. For historical analyses, the use of an ANN currently appears the most promising for the humidity correction of meteorological data. In this work, this would have required an additional intermediate step in the methodology as it is not currently implemented as a correction method in the contrail models used.

The OpenSky network has developed over the last decade and can be given access to for research purposes, free-of-charge. While it has coverage for most of the studied period and airspace, there are still some volumes of airspace that — at least temporarily — appear to lack coverage. Other networks with a larger coverage are available, albeit at a cost. It is unclear how these networks would differ in data quality. For this work, some effort has been made to clean the data, processed with the traffic library, from erroneous data points. Given that ADS-B is based on GNSS, external factors in this decade may have caused inaccuracies.

The typecode of aircraft pertaining to the flight trajectories could be determined in most cases (86 %). However, because this was the first filtering step, it is unknown how many of the flights with unknown typecodes that might otherwise have been included in the final studied dataset. The subsequent filters removed another 32 % of the remaining flights. This could therefore affect the total absolute values by approximately 10 %.

The engine type and initial mass of the aircraft are entirely unknown. The absence of engine information affects the results for typecodes differently, as the engine parameters can differ more for typecodes with engine options from several manufacturers than for typecodes with a single engine option. There are also several variations of engine types, both for different and for the same aircraft types; for example, OpenAP includes data for 80 variants of the CFM56 engine. Even if market shares were used to weight the engine parameters, contrail formation and persistency depend on the specific operating conditions of each flight. Because the market share within this dataset is unknown, such weighting would be unlikely to produce proportional results. The initial mass is also unknown, which can vary depending on route length and other operational fuelling strategies. What further affects this study, beyond using a default initial mass of 0.8 of MTOW, is the decision to only study flight trajectories with endpoints in Swedish airspace. While the mass would be the same for flights originating within Sweden, overflights and international flights with a Swedish destination would have had a lower mass if the segments of flight trajectories prior to entry into Swedish airspace had been included. Including those segments would make the data acquisition process more

complex and require more storage space as well as additional processing time. The absence of information regarding engine type and initial mass is, however, mostly a cause of uncertainty for analyses of historical data. In an operational flight planning perspective, the engine type would be specified, and the initial mass would be known to a certain degree.

Some discrepancies in the results between the contrail aCCF and CoCiP, i.e. the opposite results of warming versus cooling contrails and the variation in magnitude, could be due to the contrail aCCF assuming a fixed lifetime of six hours, while the lifetime of CoCiP contrails is dynamic. This allows for the larger variation in magnitude from the CoCiP model, and the difference in lifetime also contributes to how long the contrails exist during warming and cooling hours of the day, thus potentially giving the opposite results produced by the two models. The difference in the number of flights where contrails form according to the two models is also unexpectedly large. As previously mentioned, the developers do not recommend the contrail aCCF for use in spring, autumn or tropical regions. The results still show the same differences throughout the year. The disregard of aircraft type could also be a factor. It could also be that the implementation was not performed correctly, in addition to the decision to let the condition for persistency to depend on the SAC and not just the ISSR.

In the optimisation methodology, although Sweden has a free route airspace, it was decided to only let the altitude vary while the lateral coordinates were locked for three reasons. The first reason being the delimitation to study the effect of altitude change. The second reason being that, for overflights, it appears unrealistic to only optimise the flight within the Swedish FIR in this way, and that the entire flight (within free route airspace) should be considered otherwise. The third reason being that, for full flights, the initial and final segments of the trajectory depend on arrival and departure routes to and from airports. The initial and final waypoints of full flights were also constrained vertically for the same reason. For overflights, the initial point is seen as the origin where there is no information or control over what might have been a better alternative. It was initially attempted to keep the final waypoint vertically unconstrained for full flights. Since the fuel consumption is part of the objective function, this led to a behaviour of descending towards the final waypoint. Therefore, it was first decided to allow an altitude window around the original final altitude. Since this still allows for the descending behaviour, and the fact that future conditions along the flight trajectory are neither known nor considered, it was decided to constrain this to match the original final waypoint as well. While OpenAP.TOP also has an option to use cost index as the objective function, this work did not take a financial-cost approach to the effect of contrails. Therefore, the maximum time was constrained to 1.10 times the original time to allow for potential variations with different altitudes while also considering the temporal interest of the airlines and travellers. As seen in the results, this became an active constraint for several flights. Another improvement of the optimiser could be to constrain the speed variable in the initial control vector to match the one of the original trajectory, as that affects the initial state.

Regarding the optimisation results, it is unexpected to see trajectories in which both fuel burn and resulting EF have increased, given that both are parts of the objective function. Apart from the optimisation improvements mentioned above, there can be several reasons for this. One is the difference between the results from the trajectory and grid versions of CoCiP, where e.g. the angle of the contrail in relation to the sun can affect its lifetime and thereby also the balance between the warming and cooling effects. Another reason is the fact that two different performance models are used, OpenAP for the trajectory optimiser, and the PS-model for the contrail evaluation. Using the same performance model throughout would

require more work on the methodology, as OpenAP is implemented in OpenAP.TOP, whereas the PS-model is easily enabled for use with CoCiP.

The analysis of the historical trajectories showed that the ranges of altitudes at which contrails are created were larger in winter and spring than in summer and autumn. In the summer, about 20 per cent of flights form contrails at 33 000–34 000 feet south of 60°N, while around 10 per cent of flights form contrails at the flight levels up to 2000 feet higher or lower. In autumn, the higher-probability band rises to 36 000 feet, in spring also down to 29 000 feet, and in winter further up to 38 000 feet. It therefore appears that the results from the optimiser appear somewhat exaggerated in terms of altitude deviation, where many optimised overflights instead appear at around 25 000 feet, and full flights typically cruise at around 20 000 feet. However, the optimised results are alternative trajectories to the historical ones where contrails were indeed formed, and the large altitude deviation could therefore be a behaviour where warming contrails are avoided due to a high contrail P-ATR20 cost in comparison with the fuel burn. Using a longer time horizon for the fuel burn could lead to less extreme optimisation results.

For the discussion regarding the seasonal effects, it should be noted that the definition of the seasons in this work is centred on the solstices and equinoxes as defined in *Section 6.5*. They therefore occur earlier in the year than other common definitions for the seasons. When looking at the EF depending on time of day, it is evident that warming contrails dominate in the winter season. Flying below 29 000 feet — 25 000 in the northern latitudes — or above 40 000 feet, if possible, could therefore mitigate much of the EF contribution. In spring and autumn, the cooling effect is observed towards the end of the night into the morning. While the cooling effect dominates in the autumn, the mean EF in the spring is not clearly warming or cooling during these hours, therefore no clear rule of thumb can be derived from these results for the spring. Even if the lack of contrail formation cannot be guaranteed, flying above 37 000 feet in the autumn and spring, and below 33 000 feet in the autumn and 28 000 feet in the spring shows a lower probability of contrail formation than within these ranges. In the cooling hours of the autumn, that range could instead be preferable. The summer sees a clear cooling effect from contrails formed in the very early morning until the middle of the afternoon. To cruise at altitudes near 33 000–34 000 feet therefore appears to be preferable in the morning and during the middle of the day in summer, while higher and lower altitudes are preferred from the middle of the afternoon throughout the evening into the middle of the night. The results from the summer also show the increased cooling effect from contrails near dusk and dawn compared to the middle of the day.

As covered in *Section 5.4*, avoiding volumes in which warming contrails form increases the likelihood of conflicts with other aircraft. Altitude adjustments as a mitigation strategy may therefore be limited. Within the context of Swedish airspace, it may still be an efficient strategy north of 60°N where traffic is scarce. For flights south of 60°N and towards continental Europe, other strategies such as targeted use of SAF may prove more valuable.

This work has also given insights into how the limited supply of SAF could be distributed among flights, as a common blend for all flights is likely not optimal from a contrail mitigation perspective. If altitude adjustment is a viable strategy for domestic flights on routes heading north of Arlanda, then SAF could be more beneficial on southern routes in more crowded airspace. Turbofan aircraft flying at higher altitudes could also benefit more than turboprops operating at lower altitudes. The seasonal timeframe is likely too long to distribute SAF among seasons, however the diurnal pattern indicates that warming contrails

are more commonly formed in the latter half of the day, while cooling — or at least less-warming — contrails are found in the first half of the day. The only exception is the summer where flights in the middle of the day produce more cooling contrails. SAF could therefore be targeted at flights likely to produce warming contrails in the latter half of the day, while conventional fuel can be targeted at the first half of the day, and early afternoon in the summer. This comes with operational implications and a new dimension to fuel planning.

Building on the topic above, one future research area could be to investigate the operational feasibility of separating SAF and conventional fuel in different tanks. From a contrail mitigation perspective, conventional fuel could then be used for take-off, climb, and descent — and in cruise during the hours of day when cooling contrails form — while the SAF could be targeted for use when and where there is a high risk of producing warming contrails. A related research topic could be the effects on contrail formation from varying the speed through ISSRs. The targeted use of SAF and conventional fuel in this discussion is essentially about the characteristics of the fuel and its relation to contrail formation, and not a discussion between SAF and conventional fuels per se.

Apart from the data and methodology used for this work, the quality of the results depends heavily on the validity of the models used and current research regarding the numerous variables used within the models and the parameters that can be set. There are many factors that affect the final results, with various levels of uncertainty. From the reliability of the meteorological data, the engine design characteristics and fuel composition, the various shapes and ratios of the ice crystals produced, the accuracy of the modelling of contrail formation, advection, dissipation, and the resulting balance of EF from shortwave and longwave radiation, the effect of clouds and other contrails, the degree to which contrails contribute to global warming in comparison to e.g. CO_2 in the concept of efficacy, to how to compare the near-term effect of contrails to the long-term effect of fuel burn. While there are many uncertainties to determine the exact effect of a single flight, the currently existing and future research related to contrails and the development of mitigation strategies can provide a sufficient level of confidence to mitigate the negative effects from contrails on a large scale.

9. Conclusion

Contrails form when the combination of atmospheric conditions and the combustion of jet fuel leads to condensation within supersaturated air. Whether the combustion leads to contrail formation is determined by the SAC. The meteorological condition determining contrail formation is whether the air is saturated with regard to water. The meteorological condition determining whether contrails persist is whether the air is supersaturated with regard to ice. Persistent contrails therefore form when the SAC is satisfied within ISSRs. Depending on the balance of shortwave and longwave radiation, contrails can either contribute positively or negatively to the radiation budget of the Earth. The challenge is to determine in advance when persistent contrails form, and whether their contribution will be warming or cooling. Two open-source models that evaluate this are CLIMaCCF and CoCiP. These require meteorological data and flight performance data. In turn, the flight performance can be evaluated by the open-source model by Poll–Schumann, and by OpenAP. The accuracies of these models depend on information regarding aircraft type, engine type, fuel composition, and aircraft mass. The latter three were unknown in this work and assumptions have therefore been made. Contrail evaluation can be made for individual trajectories or on a grid. Historical flights within Swedish airspace in 2024 have been analysed with these models, and a subset of flights have been further analysed by optimising their trajectories with the open-source

trajectory optimiser OpenAP.TOP. For the optimisation, a combined objective function of the fuel burn and contrail impact has been used. The results have been analysed with regard to altitude, latitude, longitude, aircraft typecode, season, and time of day. The results from the CoCiP model were aligned with related works, while the results from CLIMaCCF showed unexpectedly low levels of contrail formation. The optimisation results proposed higher altitude deviations than expected, mostly with an improvement in EF contributions when comparing the effect of both the original and optimised trajectories as evaluated by the trajectory version of the CoCiP model. While the optimisation does not consider all factors relevant to flight operations, the analyses of the historical flights can still provide some guidance on which altitudes that are preferred or discouraged with regard to contrails in different seasons and times of day according to state-of-the-art open-source contrail models. The applicability of altitude deviations has been discussed in comparison with and in combination with the findings of related works on other mitigation strategies.

There are several prospects for future research based on findings in this work. Research into the targeted allocation of SAF, considering diurnal and seasonal variations in contrail formation as well as prevailing traffic patterns, could support the development of more effective climate-optimised fuel strategies. Further work could examine how trajectory optimisation behaves with longer time horizons for the climate metrics, or with more realistic operational constraints, which may help reduce the exaggerated altitude deviations observed in this work. Another area of interest is the influence of speed variations on contrail formation and persistency. The findings in this work would benefit with added data on engine type and aircraft mass. A more exploratory path would be to investigate the operational feasibility of separating SAF and conventional fuel into different tanks, enabling targeted use depending on the conditions for contrail formation.

This work concludes with its hours logged, leaving a contrail behind it for future research.

References

Airframes.org (2025). *Aircraft Registration Database Lookup*. *https://www.airframes.org/* [Retrieved 2025-03-10].

Appleman, H. (1953). The Formation of Exhaust Condensation Trails by Jet Aircraft. Bulletin of the American Meteorological Society, 34(1), pp. 14–20. *https://doi.org/10.1175/1520-0477-34.1.14*

Baneshi, F.; Cerezo-Magaña, M. and Soler, M. (2024). Integrating Non-CO_2 climate impact considerations in air traffic management: Opportunities and challenges. *Transport Policy*, 155, pp. 274–286. *https://doi.org/10.1016/j.tranpol.2024.06.023*

Baneshi, F.; Cerezo-Magaña, M. and Soler, M. (2025). Network-level aircraft trajectory planning via multi-agent deep reinforcement learning: Balancing climate considerations and operational manageability. *Expert Systems with Applications*, 271, 126604. *https://doi.org/10.1016/j.eswa.2025.126604*

Baneshi, F.; Soler, M. and Simorgh, A. (2023). Conflict assessment and resolution of climate-optimal aircraft trajectories at network scale. *Transportation Research Part D*, 115, 103592. *https://doi.org/10.1016/j.trd.2022.103592*

Bickel, M.; Ponater, M.; Bock, L.; Burkhardt, U. and Reineke, S. (2020). Estimating the Effective Radiative Forcing of Contrail Cirrus. *Journal of Climate*, 33(5), pp. 1991–2005. *https://doi.org/10.1175/JCLI-D-19-0467.1*

Bohman Axelsson, S.; Elneros, T. and Jerreling, O. (2025). *A Literature Survey on Aviation Contrails*. Internal ITN Report, Linköping University. Unpublished.

Bolić, T.; Gurtner, G.; Cook. A. and Soolaki, M. (2024). Can Route Charging incentivise Environmentally-friendly Trajectories? *Proceedings of the 14th SESAR Innovation Days, Rome, Italy, Nov. 2024*.

Breakthrough Energy Foundation (2025). *Specific Humidity Interpolation*. *https://py.contrails.org/notebooks/specific-humidity-interpolation.html* [Retrieved 2025-07-01]

Bräuer, T.; Voigt, C.; Sauer, D.; Kaufmann, S.; Hahn, V.; Scheibe, M.; Schlager, H.; Diskin, G.S.; Nowak, J.B.; DiGangi, J.P.; Huber, F.; Moore, R.H. and Anderson, B.E. (2021). Airborne measurements of contrail ice properties—Dependence on temperature and humidity. *Geophysical Research Letters*, 48(8), e2020GL092166. *https://doi.org/10.1029/2020GL092166*

Dietmüller, S.; Matthes, S.; Dahlmann, K.; Yamashita, H.; Simorgh, A.; Soler, M.; Linke, F.; Lührs, B.; Meuser, M.M.; Weder, C.; Grewe, V.; Yin, F.; and Castino, F. (2023). A Python library for computing individual and merged non-CO2 algorithmic climate change functions: CLIMaCCF V1.0. *Geoscientific Model Development*, 16(15), pp. 4405–4425. *https://doi.org/10.5194/gmd-16-4405-2023*

Dietmüller, S. and Simorgh, A. (2023). Dlr-pa/climaccf: Release for Reviewed GMD Paper. *Zenodo*. *https://doi.org/10.5281/zenodo.8146727*

EASA (2020). *Amendment to the Airspace Requirements on ADS-B and Mode S*. *https://www.easa.europa.eu/en/newsroom-and-events/news/amendment-airspace-requirements-ads-b-and-mode-s* [Retrieved 2025-05-30]

Eckel, F.A.; Allen, M.S. and Sittel, M.C. (2012). Estimation of Ambiguity in Ensemble Forecasts. *Weather and Forecasting*, 27(1), pp. 50–69. *https://doi.org/10.1175/WAF-D-11-00015.1*

Engberg, Z.; Teoh, R.; Abbott, T.; Dean, T.; Stettler, M.E.J. and Shapiro, M. (2025). Forecasting contrail climate forcing for flight planning and air traffic management applications: The CocipGrid model in pycontrails 0.51.0. *Geoscientific Model Development*, 18(2), pp. 253–286. *https://doi.org/10.5194/gmd-18-253-2025*

EUROCONTROL (2025). *Free route airspace*. *https://www.eurocontrol.int/concept/free-route-airspace* [Retrieved 2025-05-26]

European Commission (2025). *Reducing emissions from aviation*. *https://climate.ec.europa.eu/eu-action/transport-decarbonisation/reducing-emissions-aviation_en* [Retrieved 2025-10-16]

Falkenby, C. (2016). Luftfartssystemet & flygoperativa procedurer PPL, LAPL, 13th ed. KSAK Service AB.

FlightAware (2025). *History*. *https://www.flightaware.com/about/history* [Retrieved 2025-05-30]

Flightradar24 (2025). *About Flightradar24*. *https://www.flightradar24.com/about* [Retrieved 2025-05-30]

Gao, H. (2013). *Aircraft Cruise Phase Altitude Optimization Considering Contrail Avoidance*. (Master's thesis, Massachusetts Institute of Technology). *http://hdl.handle.net/1721.1/85768*

Gierens, K.; Matthes, S.; and Rohs, S. (2020). How Well Can Persistent Contrails Be Predicted? *Aerospace*, 7(12), 169. *https://doi.org/10.3390/aerospace7120169*

Hersbach, H.; Bell, B.; Berrisford, P.; Biavati, G.; Horányi, A.; Muñoz Sabater, J.; Nicolas, J.; Peubey, C.; Radu, R.; Rozum, I.; Schepers, D.; Simmons, A.; Soci, C.; Dee, D. and Thépaut, J-N. (2023a). ERA5 hourly data on pressure levels from 1940 to present. *Copernicus Climate Change Service (C3S) Climate Data Store (CDS).* *https://doi.org/10.24381/cds.bd0915c6*

Hersbach, H.; Bell, B.; Berrisford, P.; Biavati, G.; Horányi, A.; Muñoz Sabater, J.; Nicolas, J.; Peubey, C.; Radu, R.; Rozum, I.; Schepers, D.; Simmons, A.; Soci, C.; Dee, D. and Thépaut, J-N. (2023b). ERA5 hourly data on single levels from 1940 to present. *Copernicus Climate Change Service (C3S) Climate Data Store (CDS)*. *https://doi.org/10.24381/cds.adbb2d47*

Hofer, S.; Gierens, K.; and Rohs, S. (2024). How well can persistent contrails be predicted? An update. *Atmospheric Chemistry and Physics*, 24(13), pp. 7911–7925. *https://doi.org/10.5194/acp-24-7911-2024*

Holzäpfel, F. (2003). Probabilistic Two-Phase Wake Vortex Decay and Transport Model. *Journal of Aircraft*, 40(2), pp. 323–331. *https://doi.org/10.2514/2.3096*

Fritz, T.M.; Eastham, S.D.; Speth, R.L. and Barrett, S.R.H. (2020). The role of plume-scale processes in long-term impacts of aircraft emissions. *Atmospheric Chemistry and Physics*, 20(9), pp. 5697–5727. *https://doi.org/10.5194/acp-20-5697-2020*

Horvath, H. (2009). Gustav Mie and the scattering and absorption of light by particles: Historic developments and basics. *Journal of Quantitative Spectroscopy and Radiative Transfer*, 110(11), pp. 787–799. *https://doi.org/10.1016/j.jqsrt.2009.02.022*

ICAO (2005). Annex 2 to the Convention on International Civil Aviation. *https://www.icao.int/Meetings/anconf12/Document%20Archive/an02_cons%5B1%5D.pdf* [Retrieved 2025-03-27]

ICAO (2018). Doc 8168 Procedures for Air Navigation Services Aircraft Operations Volume I – Flight Procedures, 6th ed. International Civil Aviation Organization.

Irvine, E.A.; Hoskins, B.J. and Shine, K.P. (2014). A Lagrangian analysis of ice-supersaturated air over the North Atlantic. *Journal of Geophysical Research: Atmospheres*, 119(1), pp. 90–100. *https://doi.org/10.1002/2013JD020251*

Jensen, E.J.; Ackerman, A.S.; Stevens, D.E.; Toon, O.B. and Minnis, P. (1998). Spreading and growth of contrails in a sheared environment. *Journal of Geophysical Research: Atmospheres*, 103(D24), pp. 31557–31567. *https://doi.org/10.1029/98JD02594*

Jeßberger, P.; Voigt, C.; Schumann, U.; Sölch, I.; Schlager, H.; Kaufmann, S.; Petzold, A.; Schäuble, D. and Gayet, J.-F. (2013). Aircraft type influence on contrail properties. *Atmospheric Chemistry and Physics*, 13(23), pp. 11965–11984. *https://doi.org/10.5194/acp-13-11965-2013*

Konopka, P. (1995). Analytical Gaussian Solutions for Anisotropic Diffusion in a Linear Shear Flow. *Journal of Non-Equilibrium Thermodynamics*, 20(1), pp. 78–91. *https://doi.org/10.1515/jnet.1995.20.1.78*

Kuzmin, A.M.; Eliseev, A.V. and Mokhov, I.I. (2025). Estimates of the Tropopause Height and Its Variations Based on Reanalysis Data. *Izvestiya, Atmospheric and Oceanic Physics,* 61(1), pp. 83–91. *https://doi.org/10.1134/S0001433825700070*

Kärcher, B. (2018). Formation and radiative forcing of contrail cirrus. *Nature Communications*, 9, 1824. *https://doi.org/10.1038/s41467-018-04068-0*

Lee, D.S.; Fahey, D.W.; Skowron, A.; Allen, M.R.; Burkhardt, U.; Chen, Q.; Doherty, S.J.; Freeman, S.; Forster, P.M.; Fuglestvedt, J.; Gettelman, A.; De León, R.R.; Lim, L.L.; Lund, M.T.; Millar, R.J.; Owen, B.; Penner, J.E.; Pitari, G.; Prather, R.; Sausen, R. and Wilcox, L.J. (2021). The contribution of global aviation to anthropogenic climate forcing for 2000 to 2018. *Atmospheric Environment*, 244, 117834. *https://doi.org/10.1016/j.atmosenv.2020.117834*

LFV (2019a). *AIP SWEDEN ENR 1.3-7*. *https://www.aro.lfv.se/Editorial/View/15333/ES_ENR_1_3_en* [Retrieved 2025-03-27]

LFV (2019b). *AIP SWEDEN ENR 2.1-1*.
https://www.aro.lfv.se/Editorial/View/14268/ES_ENR_2_1_en [Retrieved 2025-03-15]

LFV (2021). *AIP SWEDEN ENR 1.7-3*.
https://www.aro.lfv.se/Editorial/View/14625/ES_ENR_1_7_en [Retrieved 2025-03-27]

LFV (2022). *AIP SWEDEN GEN 1.5-3*.
https://www.aro.lfv.se/Editorial/View/13279/ES_GEN_1_5_en [Retrieved 2025-03-27]

Lund, M.T.; Aamaas, B.; Berntsen, T.; Bock, L.; Burkhardt, U.; Fuglestvedt, J.S. and Shine, K.P. (2017). Emission metrics for quantifying regional climate impacts of aviation. *Earth System Dynamics*, 8(3), pp. 547–563. *https://doi.org/10.5194/esd-8-547-2017*

van Manen, J. and Grewe, V. (2019). Algorithmic climate change functions for the use in eco-efficient flight planning. *Transportation Research Part D: Transport and Environment*, 67, pp. 388–405. *https://doi.org/10.1016/j.trd.2018.12.016*

Martín Frías, A.; Shapiro, M.L.; Engberg, Z.; Zopp, R.; Soler, M. and Stettler, M.E.J. (2024). Feasibility of contrail avoidance in a commercial flight planning system: an operational analysis. *Environmental Research: Infrastructure and Sustainability*, 4(1), 015013. *https://doi.org/10.1088/2634-4505/ad310c*

Megill, L. and Grewe, V. (2025). Investigating the limiting aircraft-design-dependent and environmental factors of persistent contrail formation. *Atmospheric Chemistry and Physics*, 25(7), pp. 4131–4149. *https://doi.org/10.5194/acp-25-4131-2025*

Methven, J. (1997). *Offline trajectories: Calculation and accuracy* (Technical Report 44). UK Universities Global Atmospheric Modelling Programme, Department of Meteorology, University of Reading.
https://www.met.reading.ac.uk/~swrmethn/ROTRAJ/UGAMP_tech44.pdf
[Retrieved 2025-06-25]

Olive, X. (2019). traffic, a toolbox for processing and analysing air traffic data. *Journal of Open Source Software*, 4(39), p. 1518. *https://doi.org/10.21105/joss.01518*

Petty, G.W. (2008). A First Course in Atmospheric Thermodynamics. Sundog Publishing.

Petzold, A.; Neis, P.; Rütimann, M.; Rohs, S.; Berkes, F.; Smit, H.G.J.; Krämer, M.; Spelten, N.; Spichthinger, P.; Nédélec, P. and Wahner, A. (2020). Ice-supersaturated air masses in the northern mid-latitudes from regular in situ observations by passenger aircraft: vertical distribution, seasonality and tropospheric fingerprint. *Atmospheric Chemistry and Physics*, 20(13), pp. 8157–8179. *https://doi.org/10.5194/acp-20-8157-2020*

Petzold, A.; Thouret, V.; Gerbig, C.; Zahn, A.; Brenninkmeijer, C.A.M.; Gallagher, M.; Hermann, M.; Pontaud, M.; Ziereis, H.; Boulanger, D.; Marshall, J.; Nédélec, P.; Smit, H.G.J.; Friess, U.; Flaud, J.-M.; Wahner, A.; Cammas, J.-P.; Volz-Thomas, A. and IAGOS Team (2015). Global-scale atmosphere monitoring by in-service aircraft – current achievements and future prospects of the European Research Infrastructure IAGOS. *Tellus Series B Chemical and Physical Meteorology*, 67(1), 28452.
https://doi.org/10.3402/tellusb.v67.28452

Poll, D.I.A. and Schumann, U. (2021a). An estimation method for the fuel burn and other performance characteristics of civil transport aircraft in the cruise. Part 1 fundamental quantities and governing relations for a general atmosphere. *The Aeronautical Journal*, 125(1284), pp. 257–295. *https://doi.org/10.1017/aer.2020.62*

Poll, D.I.A. and Schumann, U. (2021b). An estimation method for the fuel burn and other performance characteristics of civil transport aircraft during cruise: part 2, determining the aircraft's characteristic parameters. *The Aeronautical Journal*, 125(1284), pp. 296–340. *https://doi.org/10.1017/aer.2020.124*

Poll, D.I.A. and Schumann, U. (2025). An estimation method for the fuel burn and other performance characteristics of civil transport aircraft; part 3 full flight profile when the trajectory is specified. *The Aeronautical Journal*, 129(1334), pp. 825–861. *https://doi.org/10.1017/aer.2024.141*

Ponater, M.; Marquart, S.; Sausen, R. and Schumann, U. (2005). On contrail climate sensitivity. *Geophysical Research Letters*, 32(10), L10706. *https://doi.org/10.1029/2005GL022580*

Quante, G.; Enderle, B.; Laybourn, P.; Holm, P.W.; Andersen, L.W.; Voigt, C. and Kaltschmitt, M. (2025). Segregated supply of Sustainable Aviation Fuel to reduce contrail energy forcing – demonstration and potentials. *Journal of Air Transport Research Society*, 4, 100049. *https://doi.org/10.1016/j.jatrs.2024.100049*

Rap, A.; Forster, P.M.; Haywood, J.M.; Jones, A. and Boucher, O. (2010). Estimating the climate impact of linear contrails using the UK Met Office climate model. *Geophysical Research Letters*, 37(20), L20703. *https://doi.org/10.1029/2010GL045161*

Reutter, P.; Neis, P.; Rohs, S. and Sauvage, B. (2020). Ice supersaturated regions: properties and validation of ERA-Interim reanalysis with IAGOS in situ water vapour measurements. *Atmospheric Chemistry and Physics*, 20(2), pp. 787–804. *https://doi.org/10.5194/acp-20-787-2020*

Rolls-Royce (2018). *ALECSys Lean Burn Combustor*. *https://www.rolls-royce.com/media/our-stories/insights/2018/alecsys-lean-burn-combustor.aspx* [Retrieved 2025-05-30]

Rosenow, J. and Fricke, H. (2022). When do contrails cool the atmosphere? Paper presented at the SESAR Innovation Days 2022, Budapest, Hungary. *https://www.researchgate.net/publication/366905171_When_do_contrails_cool_the_atmosphere* [Retrieved 2025-01-07]

Rosenow, J. and Köhler, S. (2024). Astronomical, Atmospheric, and Lifetime-specific Requirements for Cooling Contrails. *Proceedings of the 14th SESAR Innovation Days, Rome, Italy, Nov. 2024*.

Schmidt, E. (1941). Die Entstehung von Eisnebel aus den Auspuffgasen von Flugmotoren. *Schriften der Deutschen Akademie der Luftfahrtforschung*, 5, pp. 1–15. *https://elib.dlr.de/107948/*

Schumann, U. (1996). On conditions for contrail formation from aircraft exhausts. *Meteorologische Zeitschrift*, 5(1), pp. 4–23. *https://doi.org/10.1127/metz/5/1996/4*

Schumann, U. (2010). A Contrail Cirrus Prediction Tool. Proceedings of the 2nd International Conference on Transport, Atmosphere and Climate (TAC-2), pp. 69–74. *https://elib.dlr.de/68002/*

Schumann, U. (2012). A Contrail cirrus prediction model. *Geoscientific Model Development*, 5(3), pp. 543–580. *https://doi.org/10.5194/gmd-5-543-2012*

Schumann, U.; Baumann, R.; Baumgardner, D.; Bedka, S.T.; Duda, D.P.; Freudenthaler, V.; Gayet, J.-F.; Heymsfield, A.J.; Minnis, P.; Quante, M.; Raschke, E.; Schlager, H.; Vázquez-Navarro, M.; Voigt, C. and Wang, Z. (2017). Properties of individual contrails: a compilation of observations and some comparisons. *Atmospheric Chemistry and Physics*, 17(1), pp. 403–438. *https://doi.org/10.5194/acp-17-403-2017*

Schumann, U. and Heymsfield, A.J. (2017). On the Life Cycle of Individual Contrails and Contrail Cirrus. *Meteorological Monographs*, 58, pp. 3.1–3.24. *https://doi.org/10.1175/AMSMONOGRAPHS-D-16-0005.1*

Schumann, U.; Mayer, B.; Gierens, K.; Unterstrasser, S.; Jessberger, P.; Petzold, A.; Voigt, C. and Gayet, J-F. (2011). Effective Radius of Ice Particles in Cirrus and Contrails. *Journal of the Atmospheric Sciences*, 68(2), pp. 300–321. *https://doi.org/10.1175/2010JAS3562.1*

Schumann, U.; Mayer, B.; Graf, K. and Mannstein, H. (2012). A parametric radiative forcing model for contrail cirrus. *Journal of Applied Meteorology and Climatology*, 51(7), pp. 1391–1406. *https://doi.org/10.1175/JAMC-D-11-0242.1*

Schäfer, M.; Strohmeier, M.; Lenders, V.; Martinovic, I. and Wilhelm, M. (2014). Bringing up OpenSky: A large-scale ADS-B sensor network for research. *IPSN-14 Proceedings of the 13th International Symposium on Information Processing in Sensor Networks*, pp. 1–12. *https://doi.org/10.1109/IPSN.2014.6846743*

Shapiro, M.; Engberg, Z.; Teoh, R.; Stettler, M.; Dean, T. and Abbott, T. (2025). *pycontrails: Python library for modeling aviation climate impacts*. *https://doi.org/10.5281/zenodo.14890685*

Sun, J. (2022). OpenAP.top: Open Flight Trajectory Optimization for Air Transport and Sustainability Research. *Aerospace*, 9(7), 383. *https://doi.org/10.3390/aerospace9070383*

Sun, J. (2025). *The OpenAP Handbook*. *https://openap.dev/* [Retrieved 2025-07-03].

Sun, J.; Hoekstra, J.M. and Ellerbroek, J. (2020). OpenAP: An Open-Source Aircraft Performance Model for Air Transportation Studies and Simulations. *Aerospace*, 7(8), 104. *https://doi.org/10.3390/aerospace7080104*

Sun, J.; Olive, X.; Roosenbrand, E.; Parzani, C. and Strohmeier, M. (2024). OpenSky Report 2024: Analysis of Global Flight Contrail Formation and Mitigation Potential. *2024 AIAA DATC/IEEE 43rd Digital Avionics Systems Conference (DASC)*, pp. 1–8. *https://doi.org/10.1109/DASC62030.2024.10748832*

Sussmann, R. and Gierens, K.M. (2001). Differences in early contrail evolution of two-engine versus four-engine aircraft: Lidar measurements and numerical simulations. *Journal of Geophysical Research: Atmospheres*, 106(D5), pp. 4899–4911. *https://doi.org/10.1029/2000JD900533*

Teoh, R.; Engberg, Z.; Schumann, U.; Voigt, C.; Shapiro, M.; Rohs, S. and Stettler, M.E.J. (2024a). Global aviation contrail climate effects from 2019 to 2021. *Atmospheric Chemistry and Physics*, 24(10), pp. 6071–6093. *https://doi.org/10.5194/acp-24-6071-2024*

Teoh, R.; Engberg, Z.; Shapiro, M.; Dray, L. and Stettler, M.E.J. (2024b). The high-resolution Global Aviation emissions Inventory based on ADS-B (GAIA) for 2019–2021. *Atmospheric Chemistry and Physics*, 24(1), pp. 725–744. *https://doi.org/10.5194/acp-24-725-2024*

Teoh, R.; Schumann, U.; Gryspeerdt, E.; Shapiro, M.; Molloy, J.; Koudis, G.; Voigt, C. and Stettler, M.E.J. (2022a). Aviation contrail climate effects in the North Atlantic from 2016 to 2021. *Atmospheric Chemistry and Physics*, 22(16), pp. 10919–10935. *https://doi.org/10.5194/acp-22-10919-2022*

Teoh, R.; Schumann, U.; Voigt, C.; Schripp, T.; Shapiro, M.; Engberg, Z.; Molloy, J.; Koudis, G. and Stettler, M.E.J. (2022b). Targeted Use of Sustainable Aviation Fuel to Maximize Climate Benefits. *Environmental Science and Technology*, 56(23), pp. 17246–17255. *https://doi.org/10.1021/acs.est.2c05781*

Unterstrasser, S. (2016). Properties of young contrails – a parametrisation based on large-eddy simulations. *Atmospheric Chemistry and Physics*, 16(4), pp. 2059–2082. *https://doi.org/10.5194/acp-16-2059-2016*

Unterstrasser, S. and Gierens, K. (2010). Numerical simulations of contrail-to-cirrus transition – Part 1: An extensive parametric study. *Atmospheric Chemistry and Physics*, 10(4), pp. 2017–2036. *https://doi.org/10.5194/acp-10-2017-2010*

Unterstrasser, S. and Görsch, N. (2014). Aircraft-type dependency of contrail evolution. *Journal of Geophysical Research: Atmospheres*, 119(24), pp. 14015–14027. *https://doi.org/10.1002/2014JD022642*

Walsh, W. (2024, July 10). *Why the EU MRV on Non-CO2 Emissions Should be Voluntary.* IATA. *https://www.iata.org/en/pressroom/opinions/why-the-eu-mrv-on-non-co2-emissions-should-be-voluntary/* [Retrieved 2025-10-16]

Wolf, K.; Bellouin, N. and Boucher, O. (2024). Distribution and morphology of non-persistent contrail and persistent contrail formation areas in ERA5. *Atmospheric Chemistry and Physics*, 24(8), pp. 5009–5024. *https://doi.org/10.5194/acp-24-5009-2024*

Wolf, K.; Bellouin, N.; Boucher, O.; Rohs, S. and Li, Y. (2025). Correction of temperature and relative humidity biases in ERA5 by bivariate quantile mapping: Implications for contrail classification. *Atmospheric Chemistry and Physics*, 25(1), pp. 157–181. *https://doi.org/10.5194/acp-25-157-2025*

Yin, F.; Grewe, V.; Castino, F.; Rao, P.; Matthes, S.; Dahlmann, K.; Dietmüller, S.; Frömming, C.; Yamashita, H.; Peter, P.; Klingaman, E.; Shine, K.P.; Lührs, B. and Linke, F. (2023). Predicting the climate impact of aviation for en-route emissions: the algorithmic climate change function submodel ACCF 1.0 of EMAC 2.53. *Geoscientific Model Development*, 16(11), pp. 3313–3334. *https://doi.org/10.5194/gmd-16-3313-2023*